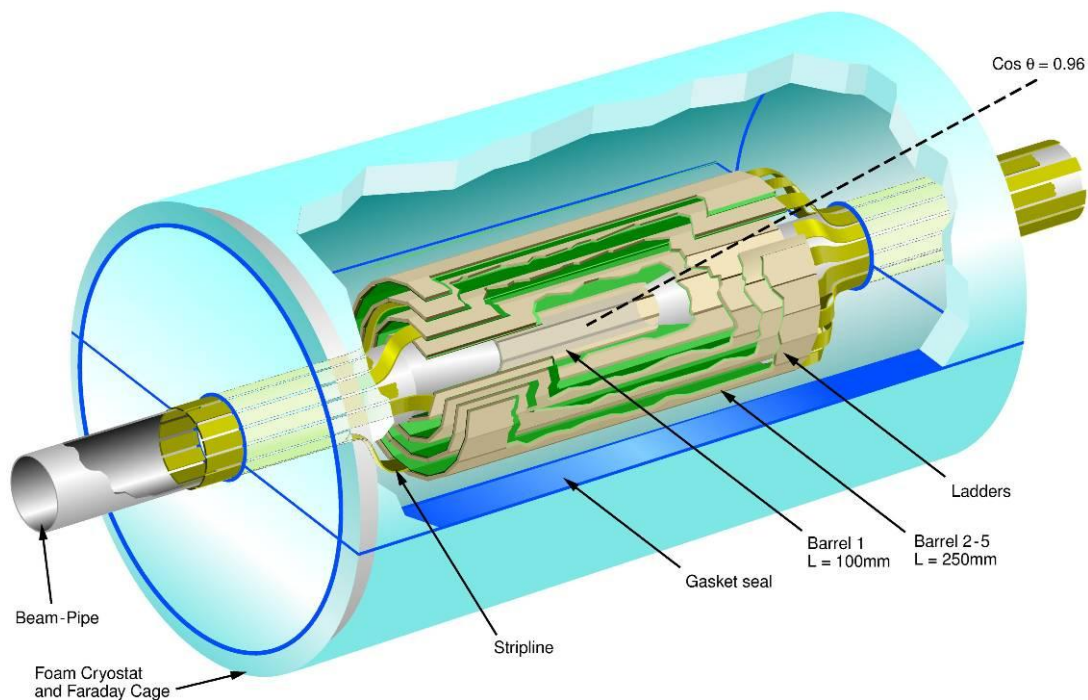


# Report on the Research Programme of the Linear Collider Flavour Identification Collaboration

October 2008



The Universities of Bristol, Edinburgh, Glasgow, Lancaster,  
Liverpool, Montenegro, Nijmegen and Oxford and the  
Rutherford Appleton Laboratory

## Contents

Introduction .....	4
WP1 – Physics Studies.....	5
Introduction .....	5
The LCFI Vertex Package .....	5
Extensions of the Vertex Package .....	6
Identification of tracks from conversions, $K_S$ and $\Lambda$ decays .....	8
Optimisation of Vertex Package parameters .....	9
Comparisons of different detector geometries .....	11
Studies of benchmark physics processes .....	13
WP2 – Sensor Design and Production .....	17
Overview .....	17
Design and manufacture of the ISIS2.....	17
Delivery of the test CCDs (CPC-T).....	19
Delivery of the last CPC2 wafers .....	20
Outlook .....	20
WP3 Readout electronics.....	21
Overview .....	21
Summary .....	21
WP4 – External Electronics .....	22
Overview .....	22
CPR2A Test Board .....	22
ISIS2 Test Board .....	22
BVM3.....	23
Outlook .....	24
WP5 – Integration and Testing .....	25
Overview .....	25
Tests of high speed CPC2 .....	25
Tests of CPR2A .....	26
Tests of CPC-T .....	28
Outlook .....	30
WP6 – Mechanical Studies.....	31
Introduction .....	31
Foam procurement and processing .....	31

New fixtures.....	32
All-silicon structures.....	33
Other work.....	34
Future plans .....	34
WP7 – Test Beams .....	35
Introduction .....	35
Results of 2007 beam test .....	35
Test beam 2008.....	37
Set-up and first results.....	38
Summary .....	41
Future Proposals.....	42
Introduction .....	42
A silicon pixel detector research programme – SPIDER.....	42
Low mass support structures for silicon detectors – LSSD .....	42
Universal flavour identification algorithms for particle physics – FLUID.....	43
Summary .....	44
Appendices.....	46
Appendix 1 – LCFI presentations.....	46
Appendix 2 – LCFI Risk Register .....	47
References .....	49

## Introduction

This document briefly describes the progress made by the Linear Collider Flavour Identification (LCFI) Collaboration since the Oversight Committee meeting in February 2008. In this period, LCFI physics studies have advanced significantly. New algorithms for quark flavour and charge identification have been introduced to the Collaboration's Vertex Package, which has also undergone extensive tuning using the most recent Monte Carlo simulations and reconstruction programs. Good progress has also been made in investigations of the capability of the LCFI vertex detector (VXD) in the context of both the SiD and ILD detector concepts. These include studies of Standard Model channels, such as measurements of the Higgs branching ratio and Higgs self-coupling, and searches for new physics, for example anomalous  $Wtb$  couplings. The international community is increasingly relying on the LCFI Vertex Package for studies of quark flavour and charge identification at the International Linear Collider (ILC).

Progress with sensor design and testing has also been good. Jazz Semiconductor has now completed the manufacture of the second generation In-situ Storage Image Sensor (ISIS) and this is awaiting delivery to LCFI. LCFI has received from e2v the test CCDs (CPC-T) which implement our ideas for capacitance reduction and low clock voltage studies. First tests of these concepts have been made using the test boards designed and constructed for this purpose and are described here.

Progress has also been excellent on the mechanical front, where new results have been obtained on the suitability of silicon carbide foam as a material for the construction of sensor ladders and perhaps the entire VXD mechanical structure, particularly regarding the machining of this material. First studies of the effects of the stresses introduced when cables are attached to the VXD have been made in the context of the "all silicon" VXD design, in which relatively thick silicon sensors are used without any support structure.

Following our first successful beam test at DESY in 2007, LCFI has carried out a second beam test using ISIS1 sensors in a pion beam at the SPS at CERN. First results from this beam test, as well as further results from the DESY beam test, are discussed in more detail in the following.

The above have been achieved despite a significant loss of manpower as a result of the STFC financial crisis. Key personnel have left the project, for example Erik Johnson, Konstantin Stefanov and Tuomo Tikkanen, while Mihai Octavian-Dima decided not to join the Collaboration.

As the current round of LCFI funding is drawing to a close, members of LCFI have been engaged in developing future programmes in the areas of sensor development, quark flavour and charge identification algorithms and their applications for future colliders and studies of novel materials for vertex and tracking detectors. These proposals are briefly described in this report.

# WP1 – Physics Studies

## Introduction

The aim of the LCFI physics studies is to guide the design of the vertex detector by assessing different detector designs, to strengthen the case for the ILC by demonstrating the physics made accessible by the collider and its detectors and to develop the tools necessary for such studies. Since the previous report, major progress has been made in all these areas.

The LCFIVertex package is being used extensively for the physics benchmark studies being performed by the ILD and SiD detector concept groups, which will lead to Letters of Intent that will be submitted at the end of March 2009. Experience with using the code is thus being gained by a wide user base as well as within the LCFI Collaboration. In the past half year, the close contact with the concept groups has resulted in further improvements to the code, partly in response to user-requests. First comparisons of different detector geometries have been taken up. The collaboration with SiD and ILD has also been vital for the work on the benchmark studies, many of which are now far advanced.

A paper on the LCFIVertex software describing the functionality and performance of the code is in preparation, with a first draft due to be circulated within the Collaboration shortly.

## The LCFI Vertex Package

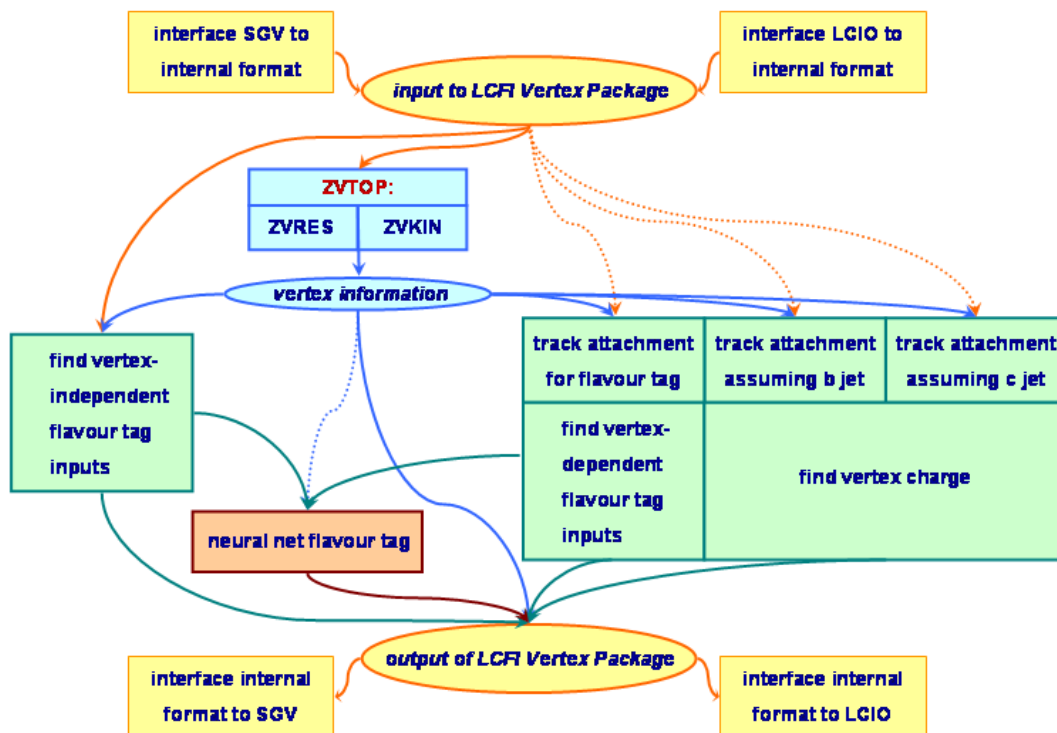


Figure 1 Structure of the LCFI Vertex Package and flow of information between the different parts of the software.

The LCFI Vertex Package is a comprehensive tool for identification of quark flavour and charge based on vertex detector information. Figure 1 shows a schematic overview of the package, input to and

output from which is handled in LCIO<sup>1</sup> format, permitting data to be exchanged between the different ILC software frameworks. The vertex finder ZVTOP provides two vertexing algorithms, ZVRES and ZVKIN (the ghost track algorithm). While the ZVRES branch is a very general algorithm coping with arbitrary multi-prong decay topologies, ZVKIN is more specialised and uses additional kinematic information. The default flavour tag procedure provided was developed for the ILC by Richard Hawkings<sup>2</sup>. It is based on nine neural networks, three each for the three cases of one, two and three or more vertices found by ZVTOP. Separate networks are used to identify b-jets and c-jets for inclusive background. For some physics processes, the background only consists of b-jets, permitting improved c-jet identification, so dedicated networks are provided for that case. For training the neural networks and obtaining the output from pre-trained neural nets, we use C++ based neural network software developed within the LCFI group. This allows flexible definition of the network architecture, e.g. number of layers and nodes, as well as variation of the transfer function and training algorithm. The LCFI package is fully interfaced to the European ILC analysis framework MARLIN, which is based on a modular approach permitting distributed code development. The common event data model LCIO allows the LCFI code to be run within MARLIN using files generated within the mainly US based org.lcsim framework and within the Asian framework (“Jupiter and satellites”). Via this route, our code is extensively employed for detector optimisation by users from the ILD and SiD detector concept groups.

### ***Extensions of the Vertex Package***

The extensions of the code described in the previous report, i.e. vertexing/flavour tagging diagnostics, the fit macro for parameters used in the calculation of one of the flavour tag inputs and a “CCD digitizer”, were released in May and August, respectively.

In preparation for the Letter of Intent (LoI) physics studies, the ILD concept group set up a centralised event simulation and reconstruction chain on the GRID. In order to reduce the time required to read in the reconstructed events from disk for further analysis, a set of output variables was defined and the file format in which these are stored was slightly modified. The resulting new “DST” format is still LCIO based, but contains a smaller number of collections, thus significantly reducing runtime overheads. In collaboration with the ILD detector optimisation group and the DESY experts responsible for the mass reconstruction, LCFI provided a set of new processors for writing and reading the LCFIVertex outputs in a way that is compatible with this new DST format.

Also in the context of the ongoing LoI physics studies, the algorithm to determine the sign of the quark charge was extended to now also cover jets for which the vertex charge is found to be zero, which is the case for approximately 60% of b-jets, and cases for which only the primary vertex is found and the vertex charge algorithm can therefore not be applied. The new JetCharge processor, developed in the context of the study of anomalous Wtb coupling, calculates a jet charge variable following earlier approaches, e.g. at PETRA, LEP and the Tevatron. The jet charge is obtained by

summing the momentum weighted charges of all the tracks in a jet, i.e.  $C_J = \frac{\sum_{i=0}^n P_i^{0.3} q_i}{\sum_{i=0}^n P_i^{0.3}}$ , where

the exponent was optimised using a sample of jets from  $t\bar{t}$  events. Possible further improvements to quark charge determination are under study.

In response to a user-request, the neural network code was extended to allow the determination of the relative importance of the various neural net inputs for a given input sample. For this purpose, the same algorithm that is used in the TMVA<sup>3</sup> package was implemented. In addition, a call to this method was added in the FlavourTag processor, which now prints out this information at the end of each run.

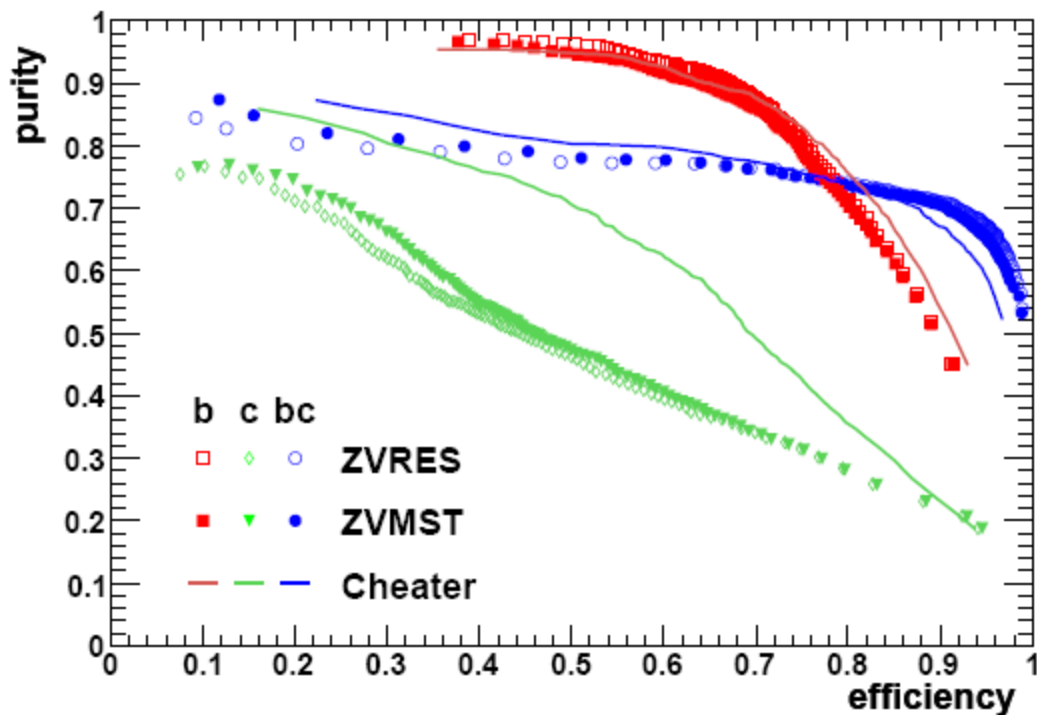


**Figure 2** Flavour tag obtained from the new vertex finding algorithm ZVMST, compared with the classical ZVRES algorithm and to a “vertex finder cheater” that uses MC information to decide which tracks to use for the vertex fits; see text.

In the course of writing the ZVTOP section of the LCFIVertex publication, an idea for a new ansatz for vertex finding was developed that combines the ZVTOP algorithm with a novel minimum spanning tree approach. In order to see if this new algorithm, named ZVMST, could lead to an improvement compared to the existing algorithms, it was implemented within the LCFIVertex code and an initial study was performed, see<sup>4</sup> for full details. Using events at the Z-resonance, ZVMST was shown to be competitive with the existing algorithms. For further comparisons, a “vertex cheater” was also implemented, which fits vertices to sets of tracks that are known from the MC record to have a common origin. These “cheater vertices” can subsequently be treated in the same way as reconstructed vertices and give an indication of the flavour tag performance that would correspond to optimal vertexing, if using the same neural networks for the flavour tag. The resulting comparison of performance for ZVMST, ZVRES and the cheater is shown in Figure 2. The new ZVMST algorithm yields an improvement of up to 5% in purity for the c-tag, while performing slightly less well than ZVRES in terms of b-tag purity. The flavour tagging performance yielded by both algorithms is very similar, while differing considerably from the results obtained from the vertex cheater. It should be noted that the results presented are preliminary. In particular, the algorithm parameters of both ZVRES and ZVMST are not yet optimised, and the study is limited to jets of energy about 45 GeV.

## ***Identification of tracks from conversions, $K_S$ and $\Lambda$ decays***

A combined processor for identification of tracks that arise from photon conversions in the tracking detectors or from the decays of  $K_S$  or  $\Lambda$  particles has been completed and the parameters of this new processor, called ConversionTagger, have been optimised using a sample of  $e^+e^- \rightarrow q\bar{q}$  events at the Z-peak. The output of this ConversionTagger processor is a copy of its input collection, in which the tracks identified to come from the above sources are removed. This output collection is then used as input to all subsequent steps, beginning with the vertexing.

Internally, all combinations of two ReconstructedParticle objects that contain exactly one track are considered. These are required to pass the following criteria to be identified as conversions or  $K_S/\Lambda$  decays:

- The constituent tracks must have opposite charge.
- The distance of closest approach between the two track-helices must not exceed 1mm, where the distance is determined using the method `GetDistanceToHelix` of the `Helix` class provided in the directory `MarlinUtil` of the `MarlinReco` package.
- The distance between the point of closest approach and the IP must be larger than 1 mm.
- The mass of the combination has to be compatible with resulting from a conversion or a  $K_S$  or  $\Lambda$  decay.

To check the mass compatibility, the rest-mass of the combination is calculated using three mass hypotheses, with appropriate choices for the constituent particle masses: for conversions both tracks are assumed to be due to electrons, for the  $K_S$  hypothesis both are assigned the pion mass and for the  $\Lambda$  hypothesis the track with the larger momentum is assigned the proton mass and the other track the pion mass. The resulting rest-mass of the combination is considered to be compatible with the hypothesis if it differs from the expected value of 0 for conversions and the PDG value for  $K_S$  and  $\Lambda$  particles by not more than 5 MeV for conversions and kaons and by not more than 2 MeV for lambdas.

The flavour tag performance obtained when the ConversionTagger is run is shown in Figure 3 and compared to the two cases that either none of these tracks have been removed by the LCFI code<sup>1</sup> or that all the tracks from these sources are removed using Monte Carlo information. As one can see, the ConversionTagger permits the removal of most of the tracks stemming from these effects resulting in a performance that is close to the optimum found using MC truth for the same purpose.

---

<sup>1</sup> Note, though, that 10% of the conversions are identified and removed from the input of our code by PandoraPFA.

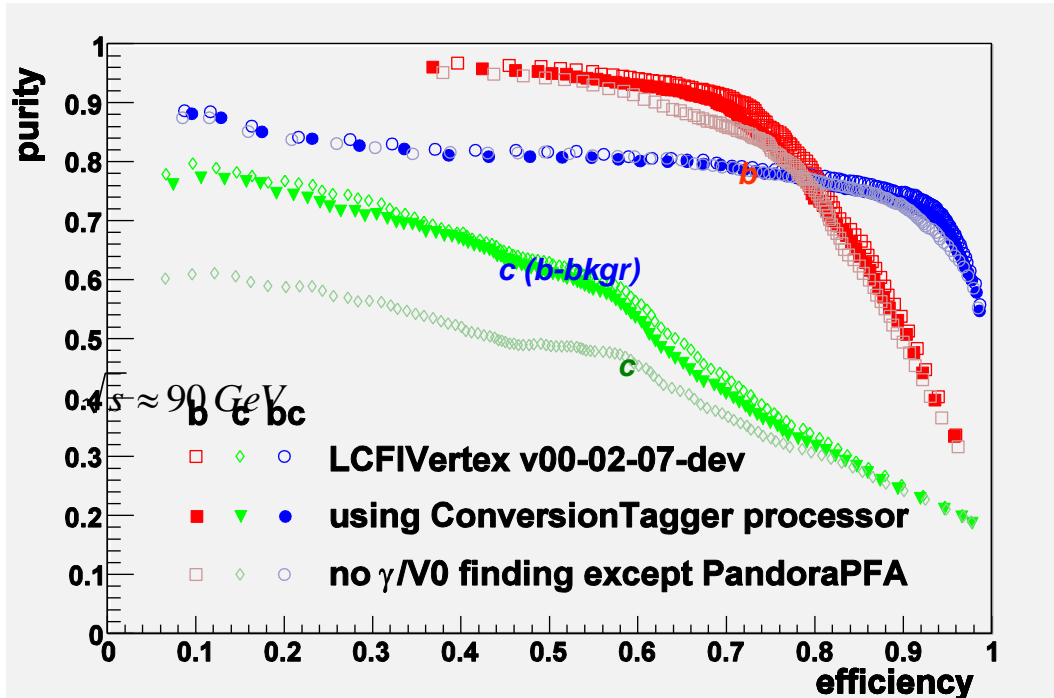


**Figure 3** Comparison of purity of the flavour tags for b-jets, c-jets and c-jets with b-background only, plotted as a function of efficiency, for a CMS energy of 90 GeV. Full symbols correspond to the result from our package when using the new ConversionTagger processor. Open symbols correspond to the performance with no correction/masking of decay tracks using MC information, see text.

### ***Optimisation of Vertex Package parameters***

The Vertex Package has a number of parameters that the user can set in the xml steering files without the need to recompile the code. As defaults for these parameters, the values that were used in the FORTRAN version of the ZVRES vertex finder and the flavour tag were initially implemented. These defaults had partly been obtained using the old BRAHMS GEANT3-based MC, which for some detector regions had problems with track linking between different subdetectors. Other default values were modified using the fast MC simulation SGV<sup>5</sup>. Both these simulation programs were run with implementations of the TESLA detector, which differs in some respects from the current baseline design envisaged for the ILD Lol. The flavour tag neural networks that LCFI provided as default with the first release are also based on these settings and the simplified reconstruction of the SGV program.

An important part of the transition to full MC and reconstruction, and the current focus of our work on the LCFIVertex code, is therefore the readjustment of these parameters and retraining of the flavour tag networks using the GEANT4-based detector simulation program MOKKA and an ILD detector model. This work is now nearing completion, using the LDCPrime\_02Sc detector model, with which the first round of benchmark studies within the ILD detector concept has been performed and which is almost identical with the model which the ILD detector concept group agreed to use for their Lol studies at a recent meeting (Cambridge, 11<sup>th</sup>-13<sup>th</sup> September).

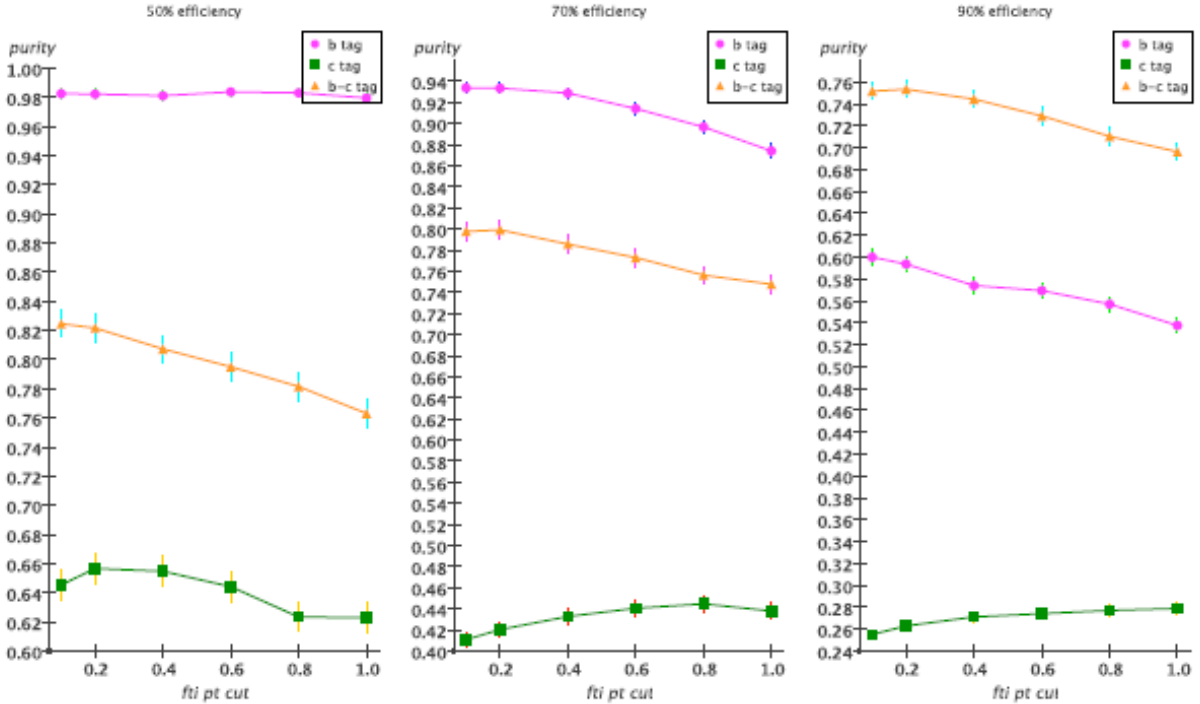


**Figure 4** Effect of varying the transverse momentum cut on the input tracks for the flavour tag variables. Shown is the purity of the three flavour tags at fixed efficiencies of 50%, 70% and 90%.

Quantities that are being optimised include three sets of track selection cuts for the fit of the event vertex, the ZVRES vertex finder and the subsequent calculation of the flavour tag inputs, three parameters of the ZVRES code and parameters for the flavour tag input variables. For each parameter, a study is made of how the flavour tag performance of the three tags at three representative efficiency values (50%, 70% and 90%) changes as the parameter is varied. A typical plot from this parameter adjustment study is shown in Figure 4, where the parameter varied is the transverse momentum cut applied to the input tracks that are used for the calculation of the flavour tag variables.

A set of new neural nets has been trained using the LDCPrime\_02Sc model and the previous set of code parameters. As the neural net performance depends on the start values for the network weights in the training run, which are chosen randomly, the training is performed several times per network and the net yielding the best performance is selected for each type of neural net. The resulting flavour tag performance is plotted in Figure 5 and compared to the previous result obtained with the same detector geometry and the neural networks obtained using a fast MC (SGV) training sample. Flavour tag purity is clearly increased for both the b-tag and the c-tag at low c-tag efficiency. At high c-tag efficiency, it is degraded with respect to the fast MC result. This is possibly due to the fact that for the training of the new networks, realistic track errors including non-Gaussian tails from multiple scattering were used, and that the ConversionTagger was run rather than using MC information to mask tracks from  $K_S$  and  $\Lambda$  decays which was done for the previous SGV training sample.

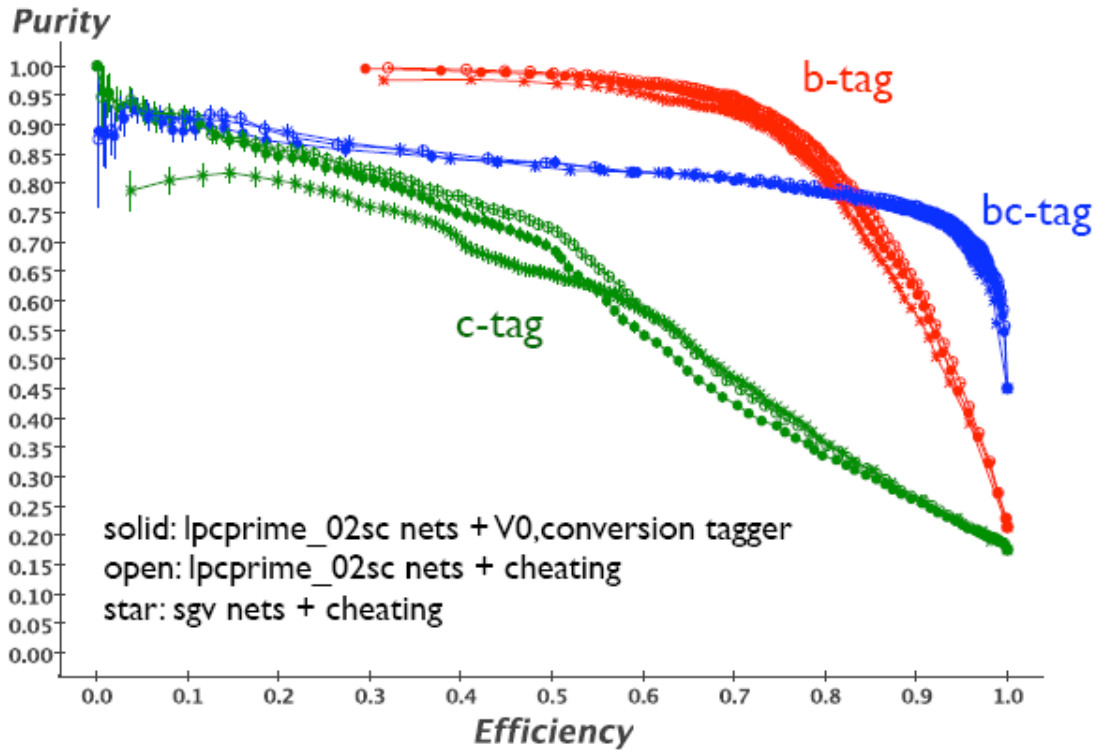


**Figure 5** Performance of LDCPrime with networks trained for that geometry and using the ConversionTagger compared to performance with MC information to mask conversion,  $K_s$  and  $\Lambda$  tracks and compared to performance using the former networks trained with fast MC (SGV) input.

## Comparisons of different detector geometries

The ILD detector concept evolved out of two existing concepts, the Asian GLD concept with an inner radius of the TPC drift volume of 44 cm and a 3 T magnetic field and the LDC concept, for which these values were 37 cm and 4 T, respectively. As a common point for detector performance comparisons, in each of the existing two software frameworks used within the ILD concept group, intermediate detectors, named GLDPrime and LDCPrime, were implemented, with detector parameters approximately the mean of those of the original LDC and GLD values.

As part of our software support for the LCFIVertex package, it was ensured that both the LDC model and the LDCPrime model yielded the expected flavour tagging results. The vertex detector is almost identical in both cases, the only differences being the inner layer radius (14 mm for LDC, 15 mm for LDCPrime) and the number of ladders on the two innermost detector layers (9 and 12 for LDC and 10 and 11 for LDCPrime; these values are chosen automatically by the MOKKA detector simulation code).

The resulting performance obtained with these two detector models is shown in Figure 6. Note that the procedure for conversion and long-lived particle decay track suppression was still under development at the time this comparison was made and was thus not used, and that the set of neural nets trained with an SGV sample was employed for the flavour tag.

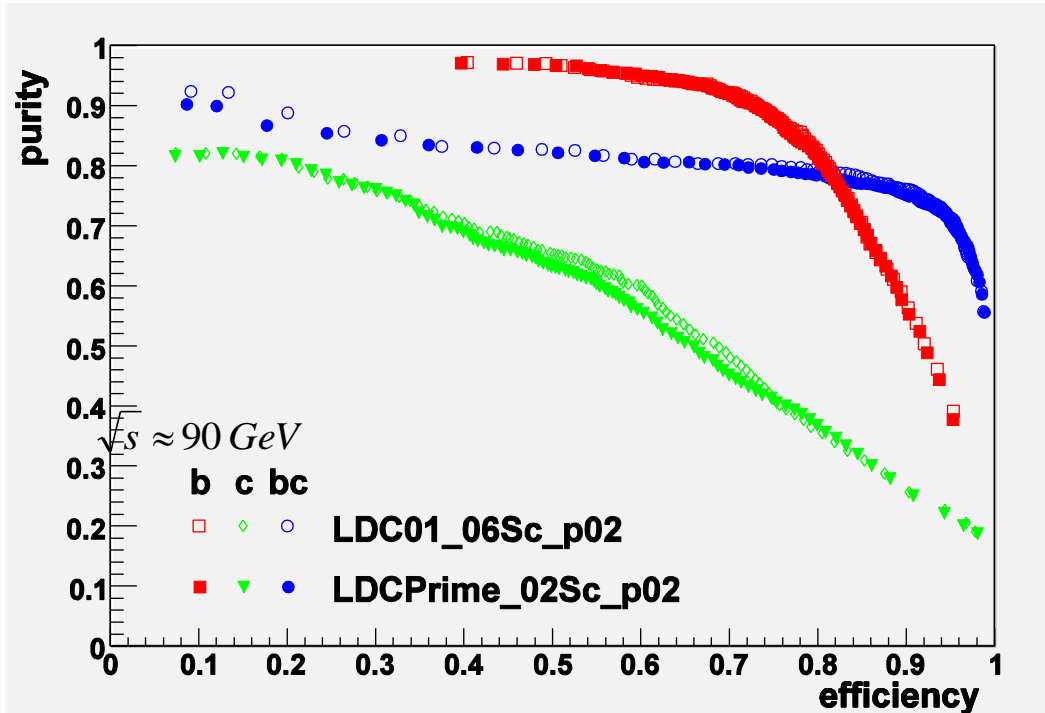


Figure 6 Comparison of flavour tag performance with the LDC and LDCPrime detector models, see text.

A significant difference between the former GLD concept and the LDC concept is the vertex detector design. While the LDC detector envisages 5 layers of sensors, the vertex detector in the GLD concept consists of three double layers, an approach that might have potential for better suppression of electron-positron pair background. At the current time, no decision has been taken on what the vertex detector for the ILD concept will eventually look like. However, the ILD group has agreed on a set of common detector parameters for the purpose of ILD benchmark studies that will form the basis of the Lol, emphasising that beyond the Lol phase the ILD detector will further evolve in response to progress in sub-detector R&D programmes.

For the Lol, the plan within the ILD optimisation group is to rerun the benchmark studies that have so far been performed with the GLDPrime and LDCPrime geometries (and partly with GLD and LDC) with this new ILD geometry. At this stage, it is also planned to replace the flavour tagging neural nets that were obtained with SGV with a new set of networks. While LCFI found significant differences between results obtained with SGV-trained nets and the flavour tag based on full MC simulation and reconstruction (see previous section), it is currently unclear if the difference between the 5 single-layer and 3 double-layer vertex detector geometries is so large that networks need to be trained with the appropriate geometry in order not to bias results.

In order to clarify this issue, and in order to help understand the differences seen between GLDPrime-based and LDCPrime-based physics studies, we are currently performing a comparison of flavour tag performance with the GLDPrime and LDCPrime geometries. For LDCPrime, the studies described above have already resulted in a set of networks trained with this geometry. For the comparison with GLDPrime, the idea is to use the same training sample at MC generator level and to pass it through the Jupiter detector simulation with the GLDPrime detector and subsequently through the “Jupiter satellites” reconstruction, plus PandoraPFA (used also for the Asian benchmark

studies), as well as the LCFIVertex package. With this training sample, networks for GLDPrime will be trained. We will then be in a position to compare the performance of LDCPrime with that of GLDPrime when using networks that are trained specifically for each of these geometries. In addition, we will be able to investigate what happens when using the GLDPrime-trained networks for LDCPrime and vice versa. If for each of the two geometries the results do not depend on which of the two sets of networks are used, then the LDCPrime-trained networks should also be usable for the new ILD detector geometry. Otherwise, it will be safer to train dedicated networks for the ILD geometry.

This work is carried out in close collaboration with KEK and Tokyo University. The GLDPrime samples were simulated and reconstructed (up to and including PandoraPFA) by Akiya Miyamoto and Taikan Suehara and made available to us via the GRID in early October. The Edinburgh GRID set-up now permits training a new set of networks within about half a week, including the latency of the GRID. Should it turn out that new networks must be trained for ILD, the MOKKA-based ILD-training samples will be provided by the DESY group.

Further work on the comparison of detector geometries has been performed in the context of the LCFI mechanical and system design studies, see the section on Work Package 6 for details.

## ***Studies of benchmark physics processes***

Processes sensitive to the vertex detector design cover the areas of Higgs physics, SUSY studies and indirect searches for new physics. The LCFI physics group has made major progress with its physics benchmark studies, in close collaboration with the benchmarking group of the SiD detector concept and the ILD detector optimisation group.

Measurement of the Higgs branching ratios, especially for the decays of a light Higgs boson into  $b\bar{b}$  and  $c\bar{c}$ , will be demanding in terms of vertex detector performance. While the study by Desch and Kuhl<sup>6</sup> was based on a fast MC simulation, with a parameterization of vertex detector performance derived from GEANT3-based full MC, LCFI is performing a new GEANT4-based study in collaboration with the ILD detector concept group, aimed at a realistic comparison of different detector designs. The leptonic channel  $e^+e^- \rightarrow ZH$ ,  $Z \rightarrow \ell^+\ell^-$  is used, as such events can be selected cleanly and because this avoids complications associated with jet-finding in multi-jet events such as wrong assignment of tracks to jets. The Bristol group has focused on the case that the final state leptons are electrons, while the Edinburgh group has focused on the di-muon channel.

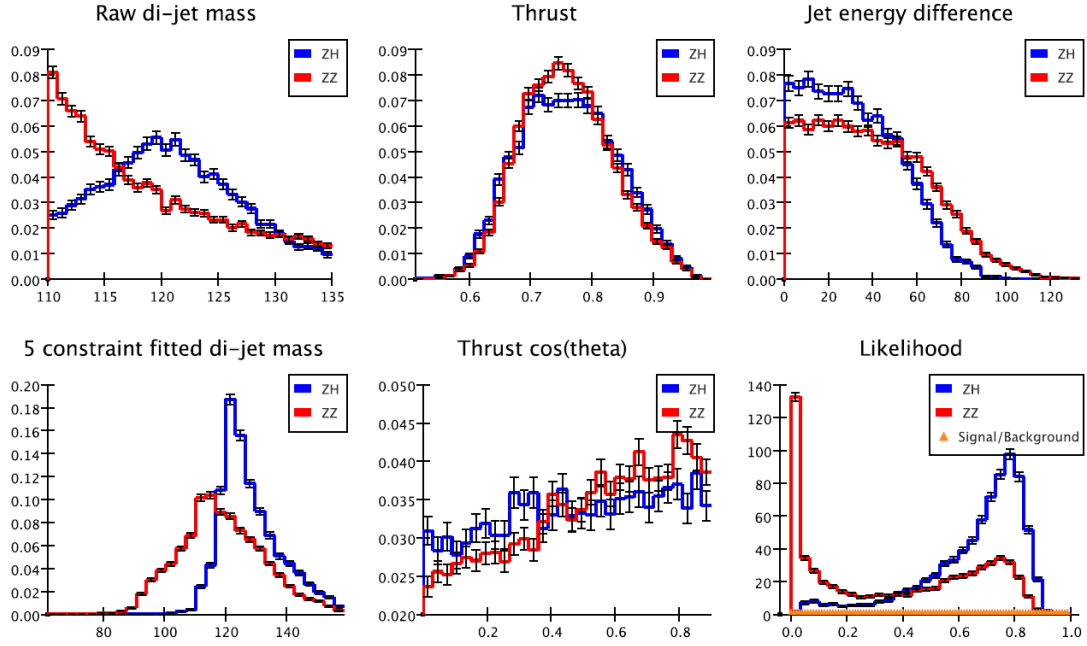


**Figure 7** Study of Higgs branching ratios: distributions of variables used in the likelihood-based event selection for ZH-signal and ZZ-background events, and of the resulting combined likelihood variable.

The experimental approach, e.g. electron-ID and event selection cuts, initially follows that proposed by Desch and Kuhl. The main event selection is based on the di-jet mass and a likelihood variable. The distributions of the quantities used to calculate the likelihood and the resulting likelihood values for the ZH signal and the main background, due to ZZ events, are shown in Figure 7. A signal to background ratio of 2.3 is achieved, compared to a value of 2.8 obtained by Desch and Kuhl.

In the future, the event selection will be revisited. In particular, it will be studied whether shifting the cut values on the selection variables can improve the selection. Further, ways of improving the likelihood-based selection by using different inputs will be explored. For the flavour tag, which is essential for extracting the branching ratios, it will be investigated if performance can be improved by using a  $k_T$ -cluster approach with fixed  $y$ -cut value, rather than forcing the event into a fixed number of jets, which tends to merge gluon-jets with one of the hadronic jets. This study of the dependence of flavour tagging performance on the jet finder configuration will also be useful for other studies performed in the ILC community.

In collaboration with the SiD detector concept group, the process  $ZH \rightarrow \nu\bar{\nu}c\bar{c}$  is also under study. Distributions of relevant kinematic variables look reasonable. The event selection efficiency remains to be studied, as do the effects of adding Standard Model backgrounds and backgrounds due to hadronically decaying Z bosons.

Major progress has been made with the study of anomalous  $Wtb$  coupling in  $e^+e^- \rightarrow t\bar{t}$ . Identification of hadronically decaying top-quarks is essential for the event selection and is achieved by requiring the missing energy to be below 50 GeV, the logarithm of the minimum  $y$ -cut to exceed 8 (when forcing the event into six jets), the sum of the b-tags for all jets to exceed 1.5, and the b-tag values of the jets with highest and second-highest network outputs to exceed 0.7 and 0.5, respectively. Two reconstructed W-bosons are required, the mass of which must lie between 65 and

95 GeV. Further event selection cuts exploit the multiplicity and mass differences between the two tops and the two W-bosons in the event.

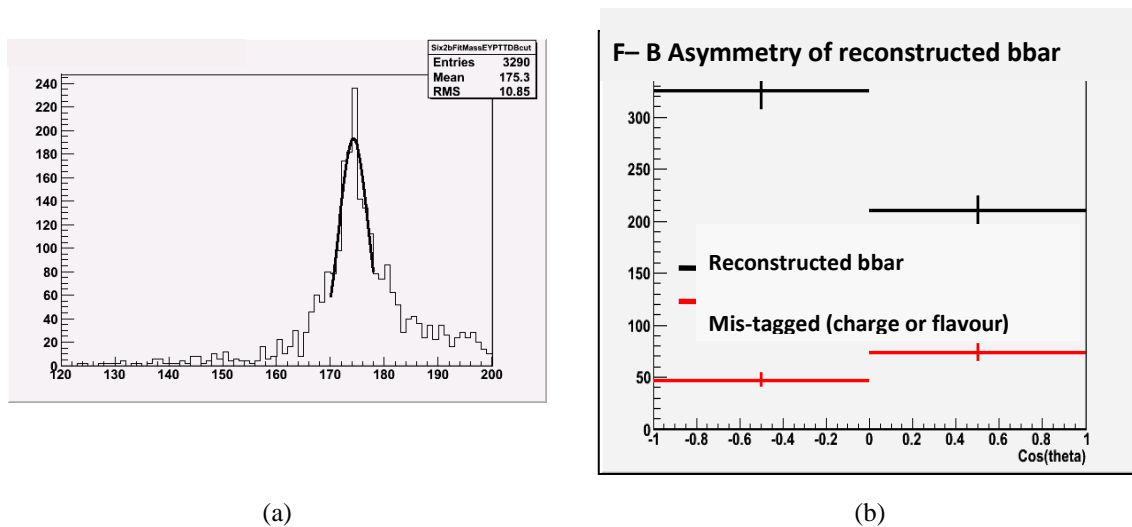


**Figure 8** Study of anomalous  $Wtb$  coupling: (a) top mass peak obtained from kinematic fit, (b) number of reconstructed  $\bar{b}$  quarks in the forward and backward regions.

The top mass is reconstructed using a kinematic fit, see Figure 8 (a). In the fit, the two b-jet candidates and the four jets corresponding to the W are first identified. The fit is performed with a W-mass constraint. The resulting top-mass peak is found to have a width of  $\sigma = 2.7$  GeV. An anomalous  $Wtb$  coupling would influence the forward-backward asymmetry of the jets stemming from the b and the  $\bar{b}$  quark. With the current approach,  $b/\bar{b}$ -jets are selected with a mis-tag rate of 2% and their quark charge is wrongly reconstructed in 19% of the jets. The number of reconstructed  $\bar{b}$  quarks in the forward and backward region is shown for correctly and wrongly identified  $\bar{b}$  quarks in Figure 8 (b). The corresponding forward-backward asymmetries are found to be  $0.33 \pm 0.07$  for  $\bar{b}$ -quarks and  $0.14 \pm 0.09$  for b-quarks, yielding a combined asymmetry of  $0.26 \pm 0.06$  (statistical errors only).

While the above results were obtained with FastMC input provided by the SiD concept group, the current emphasis of this work is on moving towards use of fully simulated events and of PFA in the reconstruction and understanding the corresponding changes in the results. Generally, results are only slightly degraded, as expected for a slightly worse resolution. A clear degradation is seen in the b-tag for uds-jets, which could be because no  $V^0$  suppression has yet been applied. To improve this study, the next step will therefore be to run the ConversionTagger developed by LCFI. Also, template mass fitting will be introduced.

The results presented in this section of the report were obtained exclusively from signal samples. Once the analysis technique has been improved as described above, the effect of adding background samples will be studied. With signal and background available, it will then be explored if the event selection can be improved by the use of electron- and muon-ID. Further work will also be required on the reconstruction of the forward-backward asymmetry, the main issues being a study of the effect of using polarised beams and of taking into account systematic effects.

Top reconstruction in the 6-jet channel has also been studied with the aim being a comparison of hit digitization as provided by the DEPFET technology and a CCD-like sensor, simulated by using the CCD-digitizer described in the previous report. No significant differences between the two sensor technologies are found for the present level of detail of the simulation.

In collaboration with the SiD benchmarking group, a study of  $e^+e^- \rightarrow ZHH$  is being performed, which aims to determine the precision with which the Higgs self-coupling can be measured in the 6-jet final state with 4 b-jets. Following the very encouraging initial results from a simple cut approach reported in February, the group is currently working on an improved event selection based on a neural net approach, following largely the method developed by Tim Barklow. Extensive signal and background samples are currently being passed through the SiD FastMC and the LCFIVertex code. With a total size of about 120 000 signal and 1.6 million background events, processing takes of order 500 hours of CPU time. These large samples will subsequently be used to train neural nets for event selection using the FANN<sup>7</sup> neural net code. This should result in a clear improvement with respect to the cut-based event selection.

## WP2 – Sensor Design and Production

### Overview

The design of the second generation In-situ Storage Image Sensor (ISIS), ISIS2 was completed in April 2008 and submitted to Jazz Semiconductor. The devices were manufactured in August and will be shipped to RAL in the next few weeks.

The Column Parallel CCD test devices (CPC-T) were delivered in March 2008 and the last four diced Column Parallel CCD (CPC2) wafers were received from e2v at around the same time.

This completes the LCFI programme of design and production of CPCCD and ISIS devices.

### Design and manufacture of the ISIS2

After discussions with several vendors, we decided that Jazz Semiconductor offers the best terms for the development of the ISIS2. Jazz Semiconductor modified one of its 0.18  $\mu\text{m}$  CMOS high-voltage processes to accommodate the required CCD buried channel and deep p+ implants. The process is 0.18  $\mu\text{m}$  dual gate oxide (1.8 V/5 V) with custom epitaxial layer (25  $\mu\text{m}$ ,  $\geq 100 \Omega\cdot\text{cm}$  on p++ substrate).

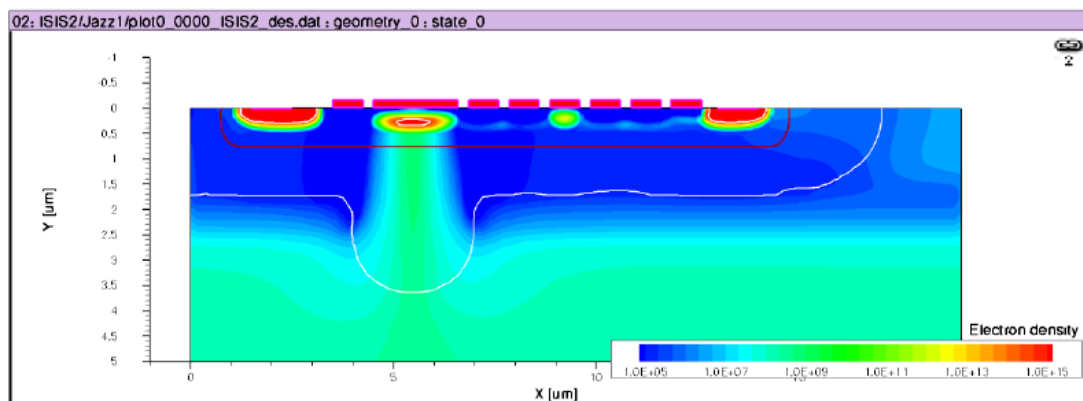


**Figure 9** Simulated charge transfer in the CCD incorporated in ISIS2 pixel for one set of dopant concentrations.

We simulated and supplied our own custom doping profiles for both the buried channel and the deep p+ implants. Figure 9 shows the simulated charge transfer for one of the variants of the buried channel.

To reduce the mask costs, we used Jazz Semiconductor's shuttle Multi-Project Wafer run. We paid for two additional masks and Jazz processed our 6 wafers independently to accommodate the custom implants. Our design used a quarter of the mask set, equal to approximately 1  $\text{cm}^2$ .

The pixel size of ISIS2 is 80 x 10  $\mu\text{m}^2$  with twenty storage cells which represents a major step forward in the miniaturization of this sensor type. The geometrical separation of the buried channel and its protection, not present in ISIS1, is a further important development, possible only at modern CMOS foundries. ISIS2 has a number of variants which will allow us to study and hence optimise the parameters for this process. They include variation of dopant concentrations, of the width of the

CCD buried channel and the presence and geometry of the deep p+ implant. Two types of reset transistors are prototyped: in the buried channel and on the surface.

The ISIS2 imaging pixel size is  $20 \times 40 \mu\text{m}^2$  while the pixel dimensions are  $80 \times 10 \mu\text{m}^2$ . The imaging pixel size is determined by the relative location of the photogates, since the charge collection occurs independently of the sensor organization above the deep p+ implant. Figure 10 illustrates the mapping between imaging pixels and physical pixels in ISIS2, where the two fold repeat was used to connect two staggered rows to one source follower at the end of the column. The total size of the ISIS2 sensor is  $5 \times 5 \text{mm}^2$ .

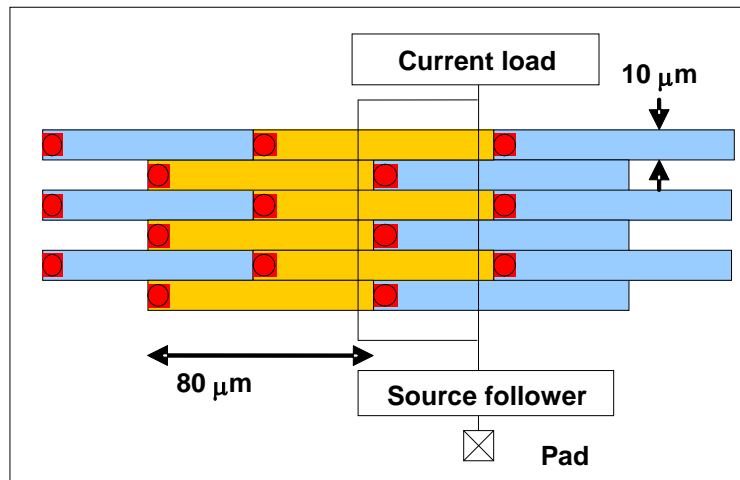


**Figure 10** The ISIS2 staggered pixel design where the red circles represent the photogates

ISIS2 will be evaluated to determine which aspects of the in-situ charge storage are critical. The goal is to understand and demonstrate the raw charge storage principle with its intrinsic immunity to noise and low power.

The channel cross section under the photogate in ISIS2 is shown in Figure 11 and the layout of the ISIS2 chip in Figure 12.

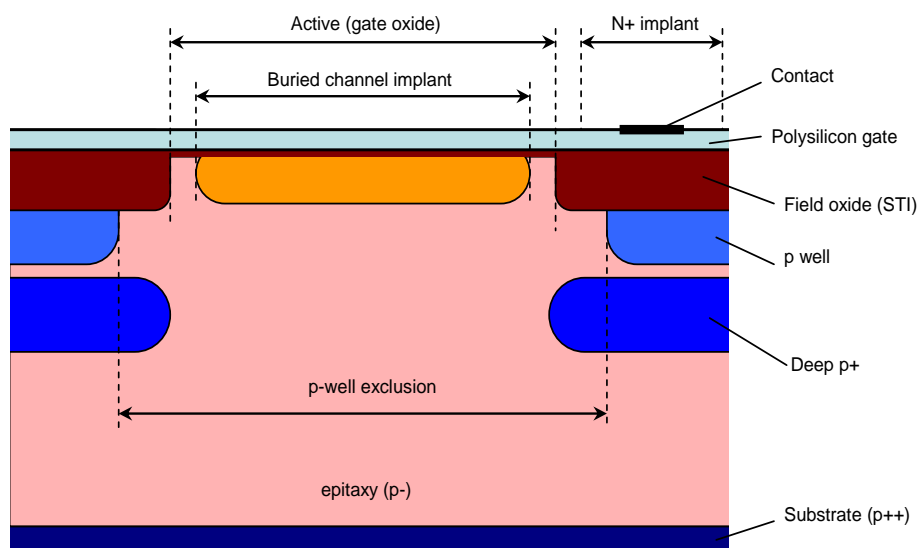


**Figure 11** The ISIS channel cross section

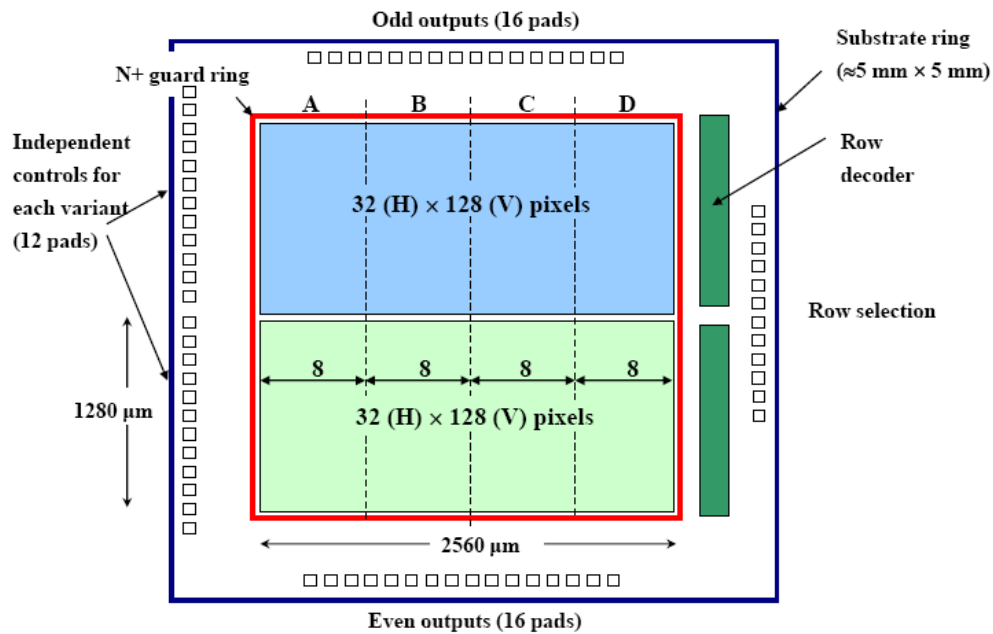


Figure 12 Layout of the ISIS2 chip.

### ***Delivery of the test CCDs (CPC-T)***

The manufacture of the 12 wafers with our CPC-T designs was completed at the end of 2007. The process and design variants we require for testing resulted in the production of 29 distinct chip types which were probed and diced at e2v. After extended delays with chip packaging at e2v, we decided to package the chips ourselves and devised procedures to do this at RAL and in Oxford. The first chips were tested in June 2008, as described in the WP5 section of this report. Figure 13 shows a picture of a section of one of the CPC-T devices.

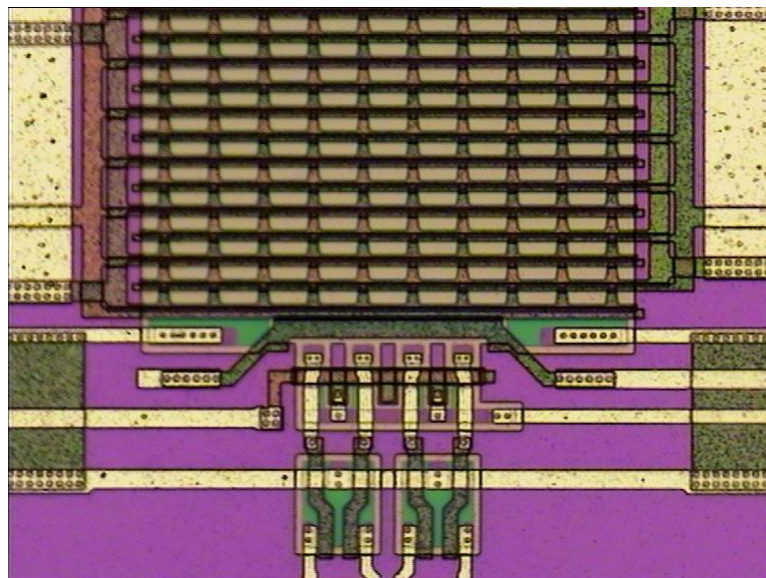


Figure 13 Photomicrograph of a section of one of the CPC-T devices.

## ***Delivery of the last CPC2 wafers***

The CPC2 order has been fully completed by e2v, with all wafers processed and delivered. The last four remaining CPC2 wafers were produced with double level metallisation and delivered to RAL. The DC testing at e2V showed that the CPC2 yield was poor. The reasons for this are not well understood. Short circuits between the two clock phases are the most common failure mode. The total count of good devices is one CPC2-70, two CPC2-40s and ten CPC2-10s. Some of these devices have already been used for high frequency tests as described in the WP5 section of this report.

Four single level metal CPC2 wafers were previously delivered to us undiced in a sealed container. These can be used in the future for bump-bonding to the readout chip CPR2A.

## ***Outlook***

The delivery of CPC-T and double level metal CPC-2 devices concludes, for this work package, the R&D programme with column parallel CCDs. A possible continuation of this direction would be the assembly of a module prototype using the high speed CPC2 with a bump bonded CPR2A readout chip and wire-bonded CPD1 driver chips.

We will seek to continue the R&D programme with the ISIS, as is discussed in the section of this report which describes proposed future research directions. The experience with the design, manufacture and testing of ISIS2 has given us important guidance in this new R&D programme.

## WP3 Readout electronics

### **Overview**

The focus in the last few months has been the support of the tests of the CPR2A column parallel readout chip, the results of which are described in the WP5 section of this report. However, it is helpful to review the results so far, with reference to the expected performance of the CPR2A.

The main changes between CPR2 and CPR2A are summarised below.

- Extension of digital functionality to provide better cluster finding efficiency.  
The test results confirm that the CPR2A works well with higher levels of occupancy. A wide range of cluster sizes and separations can be read out.
- Improvements in amplifier offset and gain matching.  
The preliminary results demonstrate good linearity and uniformity. The measurements are based on signals injected into the calibrate circuit, a new feature of the CPR2A, which makes it much easier to characterize the performance of individual channels. The outputs are taken directly from the ADC, but work is already underway to measure the analogue performance with the full cluster finding logic in operation.
- Stabilization of power supply current.  
The evidence so far is that the charge amplifiers are behaving correctly, certainly in the calibrate testing with direct ADC output. CPR2 suffered from noise injection onto the charge amplifiers, probably due to power supply transients and fluctuations. Circuit changes in CPR2A appear to have successfully reduced these fluctuations. Further work is needed to check that analogue performance is maintained for the charge amplifiers when the CPR2A operates in cluster finding mode.

### **Summary**

We have confirmation from initial testing that the performance improvements expected from the CPR2A have been successfully achieved. Work will continue on the analogue testing with cluster readout, to check that the performance is maintained when there is additional digital noise. The indications are that the CPR2A would be viable as a readout ASIC for CPCCDs in the bump-bonded configuration, both for voltage mode and charge mode amplifiers. This is a significant step forward from previous column parallel readout designs, which have had performance limitations that would have prevented their use in a detector.

## WP4 – External Electronics

### Overview

The main emphasis of this work package since the last report was on the design and production of the ISIS2 test board and the BVM3 sequencing and data acquisition module.

### CPR2A Test Board

The CPR2A test board was designed at RAL and manufactured in April 2008. This board has been successfully used to test the CPR2A chip since June 2008. A photograph of the CPR2A test board is shown in Figure 14.

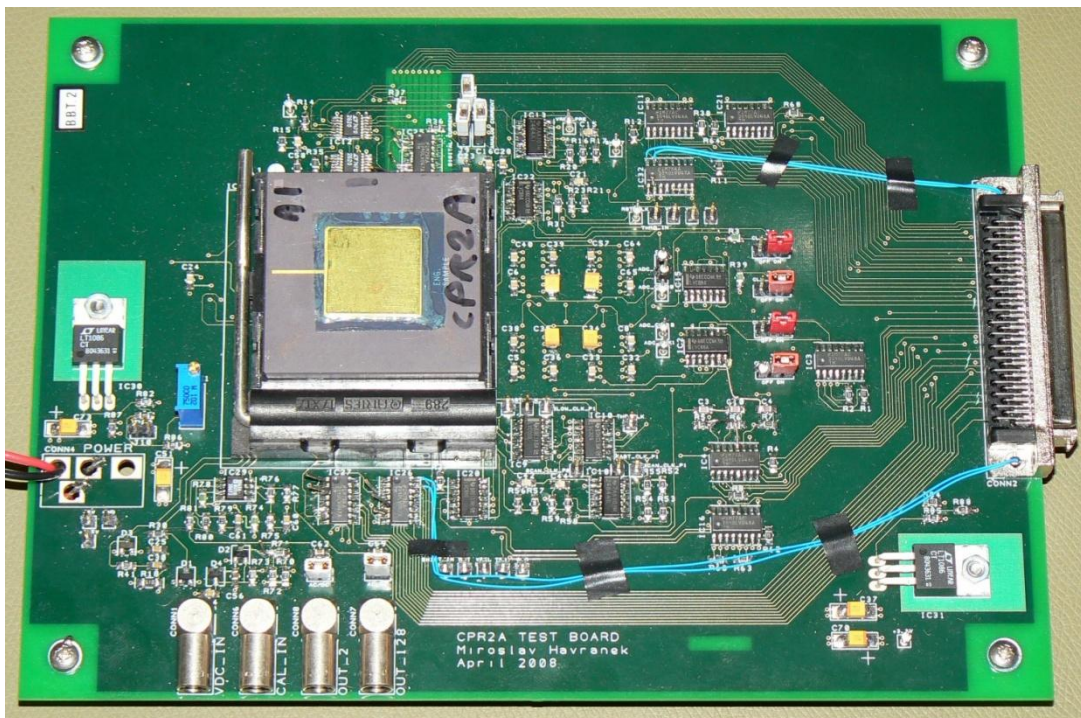
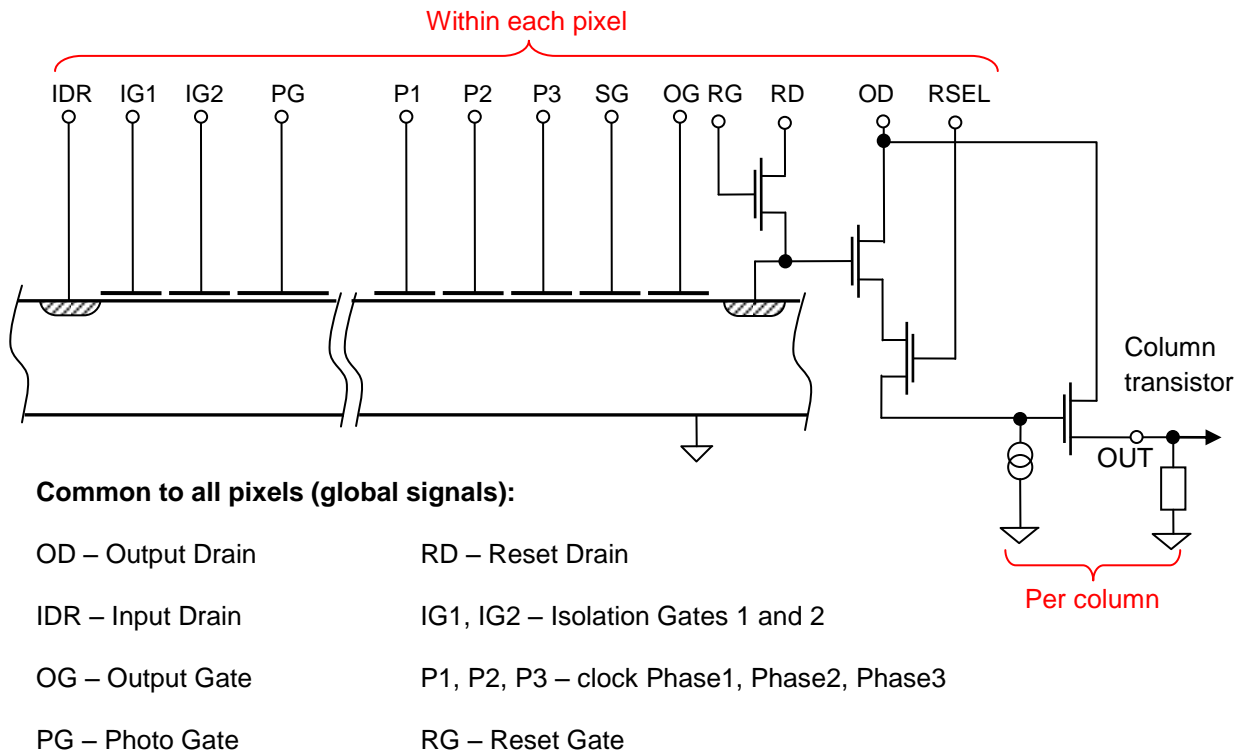


Figure 14 A photograph of the CPR2A test board.

### ISIS2 Test Board

The ISIS2 test board was designed at RAL and manufactured in September 2008. Figure 15 illustrates the input/output provision for the ISIS2 chip. The test board, which allows the full functionality of the ISIS2 to be exercised, can be controlled by the BVM2 or BVM3 modules and is connected to these using two flat cables and a transition board in the same manner as all the latest LCFI test boards.



**Figure 15** A diagram of an ISIS2 pixel showing the signals needed to steer the sensor.

The first test board has been assembled and is currently undergoing tests at RAL. Figure 16 shows photograph of the assembled ISSI2 board.

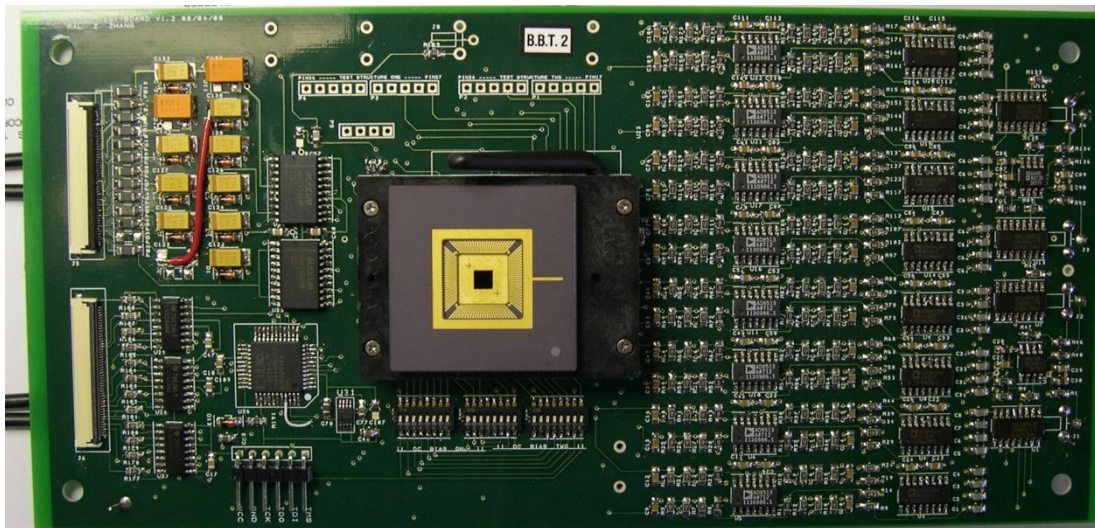


**Figure 16** Photograph of the fully populated ISIS2 test board.

### **BVM3**

The BVM3 is a considerably improved version of the BVM2, a VME-based sequencer module which is used in all LCFI test stands. The design of the module was completed in June 2008. The BVM3 has a main clock that can run at speeds of up to 100 MHz and significantly improved clock management that allows clock synchronization between multiple BVM3 devices in a beam test. It uses a Xilinx

Spartan 3A-1400 FPGA, which offers up to 502 user I/Os with various I/O standards and a 320 MHz clock speed, combined with a 32-Mbit Xilinx Platform Flash chip to allow multi-booting for 4 different firmware pages. 4M x 16 bits SRAM is used instead of the 2 M x 16 bits on the BVM2, allowing the programming of longer time sequences and the storage of larger data volumes. The main I/O port of the BVM3 is a 32-pair LVDS I/O through a SCSI connector to drive the motherboard, and more LVDS signals are available via a daughter-card. A TTL port is also available on the front panel through an IDC/LEMO connector.

The first BVM3 module, a photograph of which is shown in Figure 17, was assembled in Oxford in August 2008.



Figure 17 A photograph of the first fully populated BVM3 board.

## Outlook

The DAQ system based on BVM3 sequencer modules will be used for the continuation of the ISIS R&D programme including the ISIS2 tests using the LCFI ISIS2 test board.

## WP5 – Integration and Testing

### Overview

High-speed tests of the double level metal CPC driven by the column parallel drive chip CPD1 have been carried out in Oxford and studies made of the maximum achievable clock frequency.

Testing of the CPC-T has started at both RAL and Oxford, and several variants of the CPC-T have been evaluated. The reduction in the intergate capacitance of the tested devices was appreciable, but not as large as the maximum values that we had hoped to achieve.

Tests of the column parallel readout chip CPR2A started at RAL in May 2008: first results are encouraging.

Irradiation studies have been postponed due to the loss of testing manpower.

### Tests of high speed CPC2

The high speed double level metal CPC2 sensors were delivered to LCFI in March 2008. These sensors have the so-called bus-line free design, in which metal layers covering the whole surface of the sensor are used to distribute the clock signals. This approach minimizes the resistance in the two clock phase circuits.

Two CPC2-10 and two CPC2-40 sensors with CPD1 drivers on a MotherBoard 5.0 were prepared and tested. The CPC2-10s were successfully operated at clock frequencies of up to 35 MHz and showed good performance with a noise level of about 80 electrons for frequencies up to 25 MHz. The performance at high frequency was limited by the clock feed-through effects described in the previous report. Figure 18 shows the CPC2-10 noise as a function of the clock frequency.

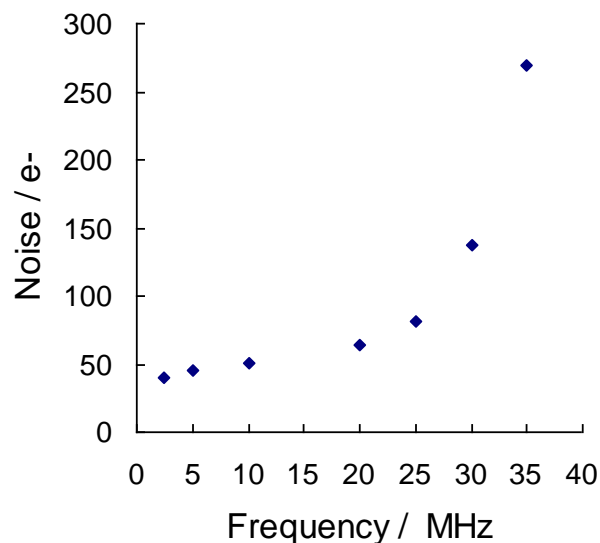


**Figure 18** Noise in electrons as function of frequency for the CPC2-10 sensor.

An  $^{55}\text{Fe}$  X-ray source was used for the tests, with the sensor operating at  $-40\text{ C}$  to reduce the dark current. Noise levels were studied as a function of a number of parameters. One example, a study of the dependence of the noise on the clock voltage with various numbers of CPD1 sections enabled, is shown in Figure 19.

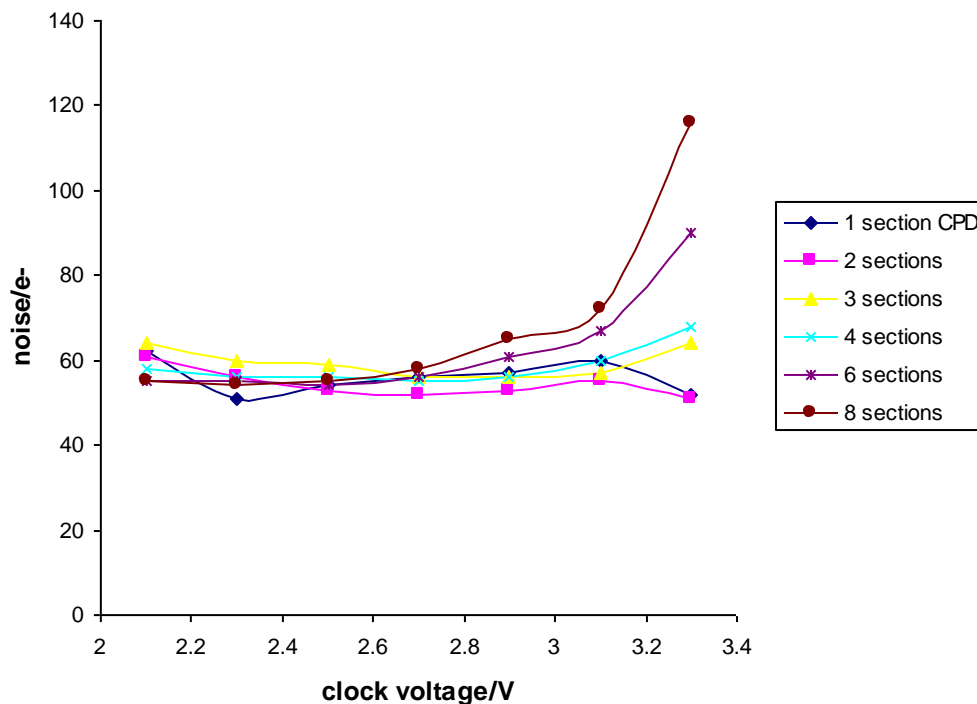


**Figure 19** Dependence of the noise in the CPC2-10 on the clock voltage for various numbers of enabled CPD1 sections.

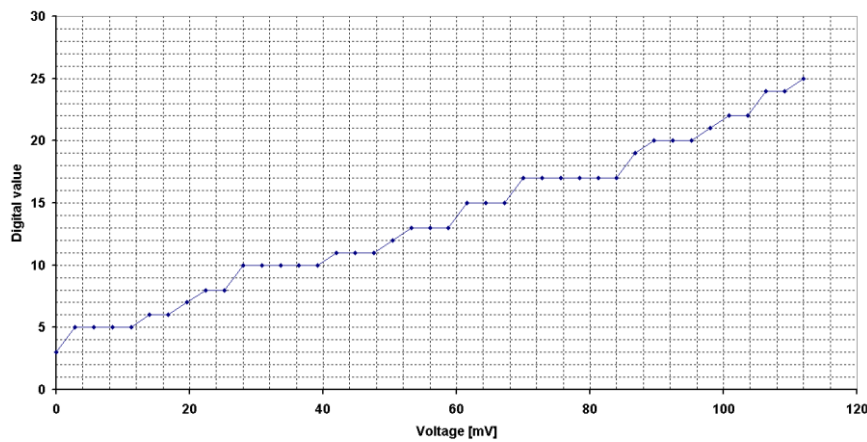
Two CPC2-40 sensors have been wire bonded for testing. One of these developed a short between the two clock phases and became unusable. The second is currently being studied in Oxford.

### **Tests of CPR2A**

The CPR2A readout chip is an improved version of the CPR2. LCFI received the CPR2A chips in April 2008 and are studying them using the CPR2A test board.

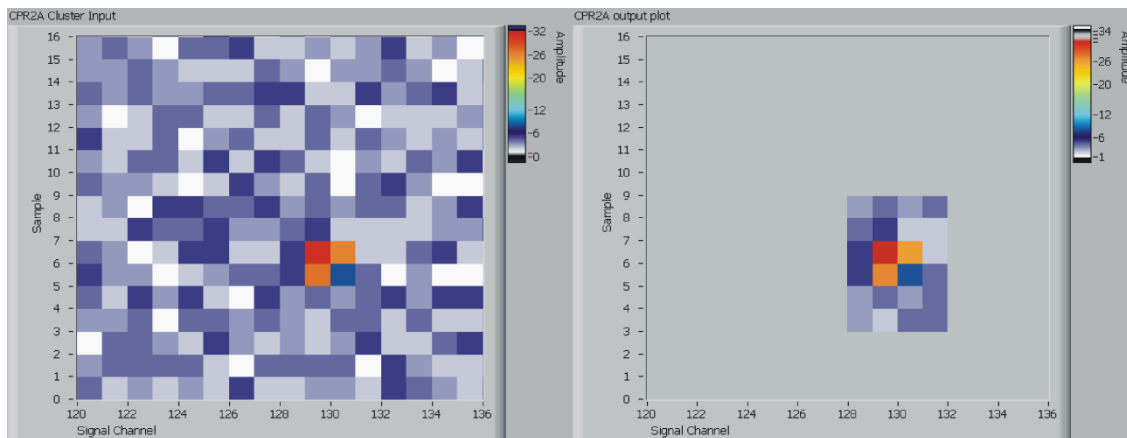
A standalone CPR2A chip allows, through a wire bond connection, a test signal to be fed to one of its inputs. By configuring the calibration and scan registers appropriately, this channel can be tested without connection to a CPC. Using this technique, we verified the functionality of the CPR2A and determined that both voltage and charge channels performed as specified. This is a big step forward since the charge inputs of the CPR2 did not work at all. Both the voltage and charge amplifiers are seen to provide good amplification and linearity. The noise level for the voltage channels was  $\pm 1$  LSB at 200 mV reference voltage. In the case of the charge channels, the noise was about  $\pm 3$  LSBs at 100 mV reference voltage. All measurements with analogue circuits were performed using a 1 MHz clock. At higher frequency, the noise increases. This effect is under investigation.

Figure 20 shows the digitized output of CPR2A as the input voltage is varied for one of the channels with charge amplification. This plot corresponds to the reference voltage of 100mV. The reference voltage determines the dynamic range of the ADC.



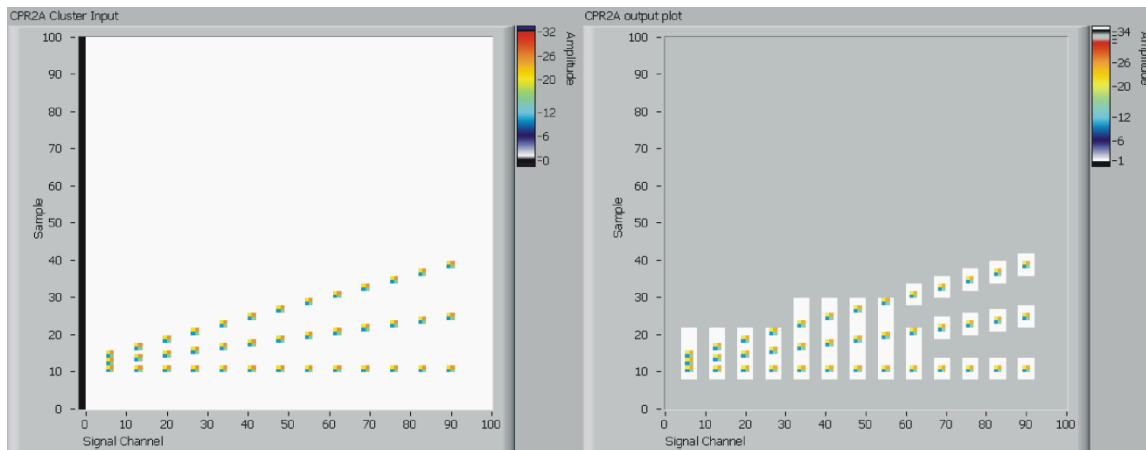
**Figure 20** Transfer characteristics of one charge amplifier coupled to an ADC ( $V_{ref} = 100$  mV).

In order to allow testing of the cluster finding logic, the amplifiers were switched off and data was fed into the cluster finder in the chip from the scan register. Specially developed LabVIEW code was used to generate the test data, which was loaded into the CPR2A. The processed data, that is, after cluster finding, was read back and the results compared with the expectations obtained by running the cluster finding algorithms off-chip. The response of the cluster finder was studied for a range of hit densities and configurations of input clusters. Figure 21 shows an example of a cluster surrounded by random noise. The left plot is the generated input and the right plot is the output from the CPR2A on-chip cluster finder.



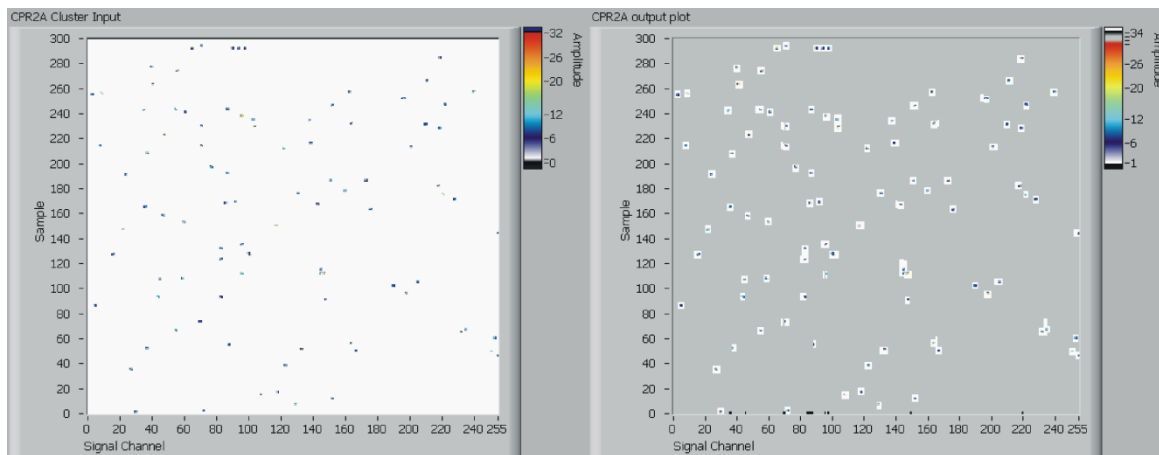
**Figure 21** Cluster surrounded by random noise. The left plot is the generated input and the right plot is the output from the CPR2A on-chip cluster finder.

Figure 22 shows the response of the CPR2A to clusters with variable vertical separation and shows how the clusters are merged into one data packet as their separation decreases. This feature of the cluster finding logic allows the reduction of the amount of data that must be transferred from the readout chip to the DAQ system.



**Figure 22** Test of CPR2A response to varying cluster separations in one column.

Finally, Figure 23 shows the performance of the CPR2A chip with a random occupancy of 0.5%. The number of errors observed in the reconstructed data is small, demonstrating that the chip is able to cope well with this level of occupancy.



**Figure 23** A section of the input frame with 0.5 % occupancy (left). Very few errors appear in the reconstructed data (right). The columns with errors are marked by black dots above the horizontal axis.

These tests indicate that the cluster finding logic is considerably improved with respect to that on the CPR2 chip. The CPR2A cluster finder is able to successfully read out both more complicated cluster shapes and a higher cluster density than that of the CPR2. As expected, some errors appear at higher cluster densities.

While the testing is yet to be completed, it is already clear that the CPR2A functions as hoped. The next step will be to test a CPR2A connected to a CPC2.

## ***Tests of CPC-T***

The CPC-T devices are small four-phase CPCCDs which were designed to allow investigation of the minimum power levels necessary to readout column parallel CCDs. In particular, efforts were made to reduce both the inter-gate capacitance and the clock amplitude necessary for efficient charge transfer. LCFI received the CPC-T devices in April 2008 after a considerable delay caused by problems with packaging the chips at e2V. In order to speed up the testing procedure, chip packaging

procedures were developed by LCFI and the packaging was finally performed at RAL and Oxford. The testing of CPC-T then started in June 2008.

First results of the investigations of the necessary clock amplitude are presented in Figure 24. This shows the dependence of the charge transfer inefficiency (CTI) on the voltage difference between the two gates which belong to the same phase (OPV). The CTI starts to grow when the difference is either too small or too large. The operational region is centred round the value of the clock amplitude, as expected.

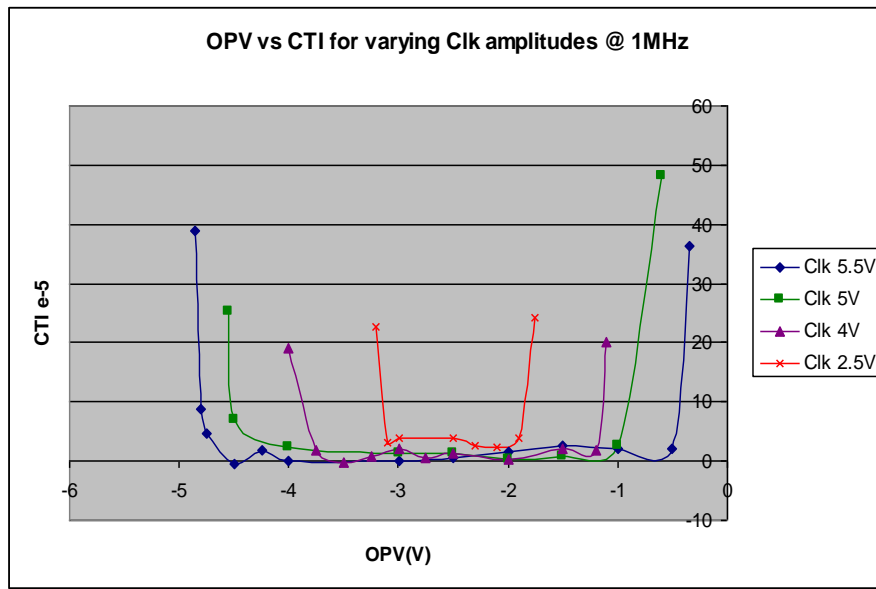


**Figure 24** Study of CTI as a function of OPV for various clock amplitudes.

Work has started to systematically characterize all 29 types of CPC-T. The measurements made include the CTI at various frequencies and the inter-gate capacitance. The current status of these studies is summarized in Figure 25.

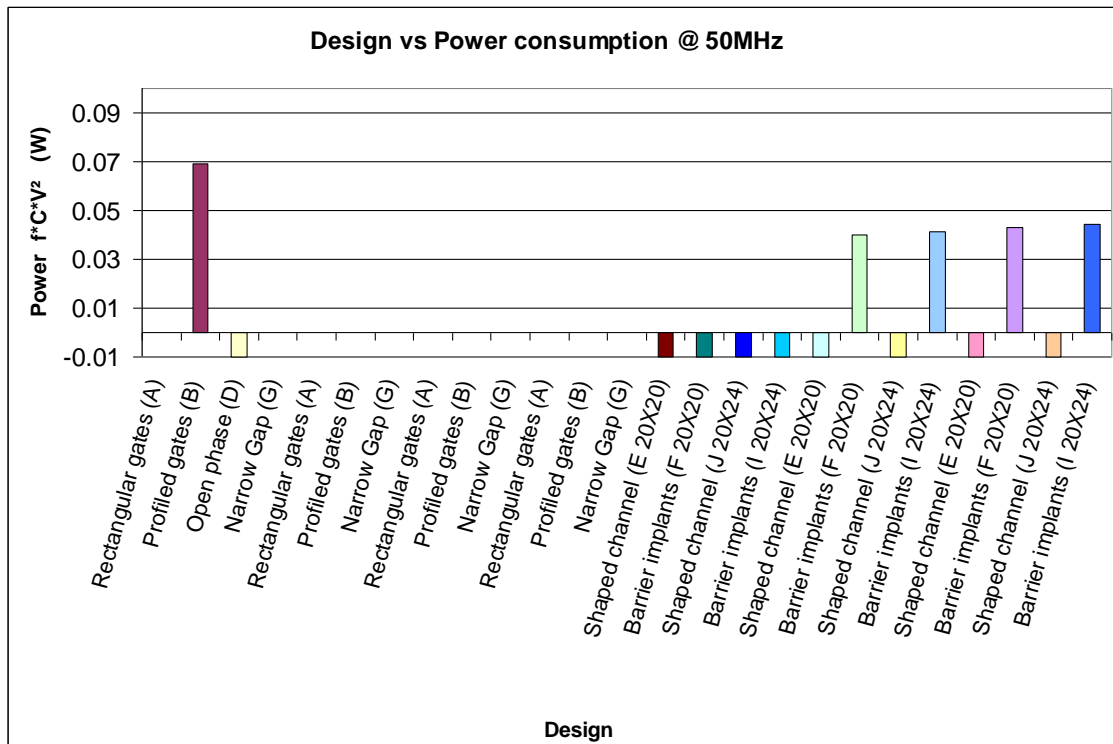


**Figure 25** Status of CPC-T measurements: positive values indicate the power consumption of the design in question at a clock frequency of 50 MHz, negative values indicate that the design did not function.

## Outlook

LCFI has successfully completed a large proportion of all major components of the column parallel CCD programme with the most recent efforts involving studies of the high speed CPC2 sensors, the reduced capacitance CPC-T test CCDs and the CPR2A readout chips. The good performance of the CPR2A qualifies it to be used with the high speed CPC2.

The reduced testing effort due to the loss of manpower has slowed down the progress in the testing, however, and has prevented us performing the proposed radiation hardness studies.

## WP6 – Mechanical Studies

### *Introduction*

Mechanical work since February has focused on understanding basic foam properties, procuring new lower mass materials, commissioning new high-precision ladder-building fixtures and training new personnel after the loss of Erik Johnson.

### *Foam procurement and processing*

Following the success of basic grinding of 6% relative density silicon carbide (SiC) foam, more challenging machining has been attempted. The test piece shown in Figure 26 demonstrates curved edges, cut-outs and drilled holes made with diamond tools. The complex shapes required for an integrated all-SiC vertex detector structure are clearly possible, although very thin “walls” do not survive, as is demonstrated by the three holes close to the bottom edge of the test piece which have run together.

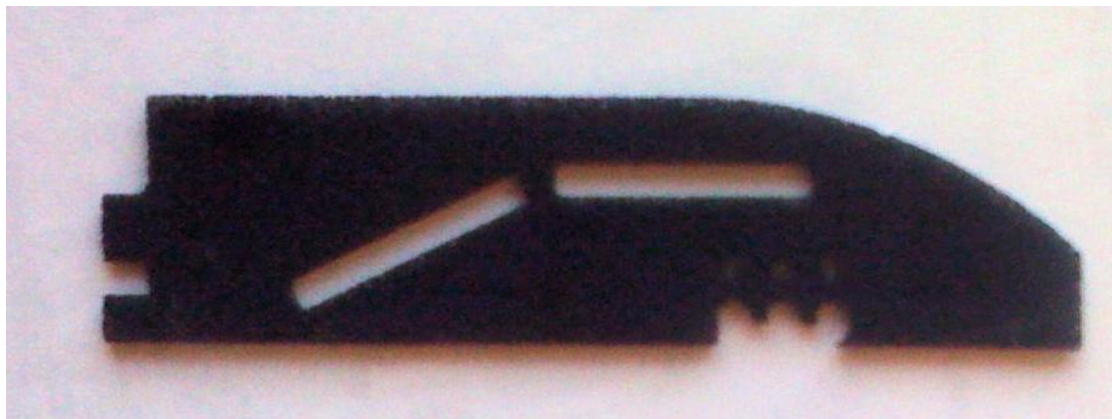


**Figure 26** A photograph of a piece of SiC foam following tests of the machining of curved surfaces, holes and slots.

We have now obtained SiC foam samples with an even lower relative density. This was nominally 2...4%, though LCFI measurements gave actual values of 3...5%. The first set of these samples is being thinned to 1.5 mm for prototype ladder building.

Samples of compressed reticulated vitreous carbon (RVC) foam have been studied. These are stiffer and easier to machine than normal RVC, but with the penalty that they are of higher density. No advantage is apparent in using this foam so it will not be studied further.

A selection of SiC and RVC foams have been given to the RAL Novel Materials group where accurate measurements of material properties such as Young's modulus, Poisson's ratio, isotropy and moisture absorption will be performed.

Close co-operation with the RAL metrology group has given us access to powerful new tools such as a travelling microscope which is being used for detailed studies of the structure of foams and the behaviour of glue pillars attached to foams, as shown in Figure 27.

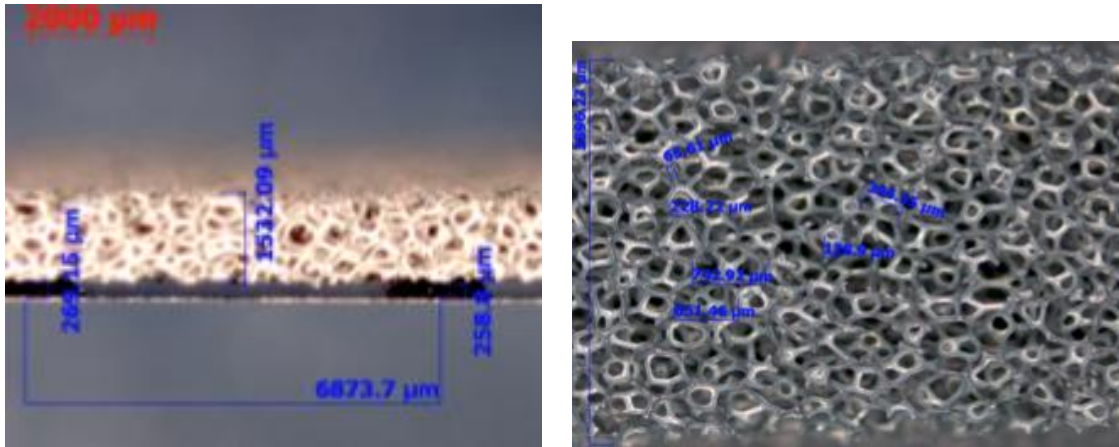


**Figure 27** Photomicrographs of SiC foam on glue pillars (left) and of the structure of SiC foam (right) illustrating measurements such as the height of the glue pillars and the size of the foam cells made using the travelling microscope.

Quotes for larger and more complicated SiC foam structures have been obtained. Half-cylinders of 30 cm length can be purchased for less than £ 2 k each. Research on such structures is the subject of a new proposal involving members of the LCFI Collaboration, as is discussed in the section on future proposals in this document.

### ***New fixtures***

We have purchased and commissioned new ladder-building fixtures which consist of two granite blocks containing ceramic foam inserts. The inserts act as vacuum chucks. Measurements by the RAL metrology group have shown the flatness of the ceramic chucks to be better than 10 μm. A photograph of the fixtures is shown in Figure 28 and the measured profile in Figure 29.



**Figure 28** A photograph of the new ladder-building fixtures showing the two granite flats with their ceramic foam inserts.

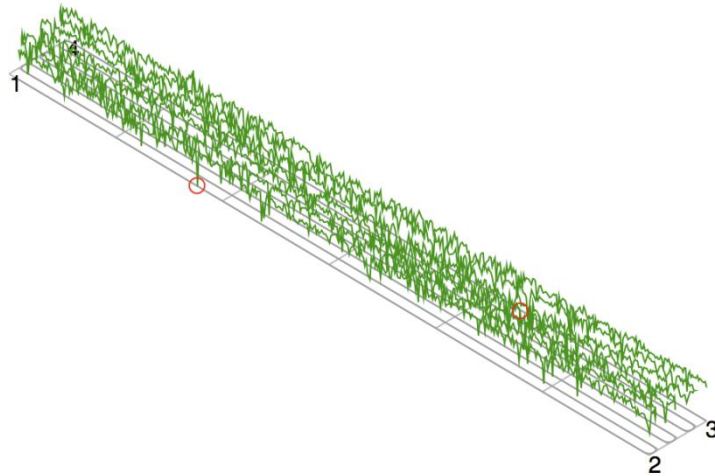


**Figure 29** Profile of the ceramic inserts in the new ladder construction fixtures. The highest and lowest points on the surface are shown by the red circles and differ in height by 8.5  $\mu\text{m}$ .

Test ladders have been built using the new fixtures. The new ladders have been tested in the cryogenic survey system, and a sample result showing the shape change of a SiC foam-based ladder over a temperature range of 25 C is shown in Figure 30.

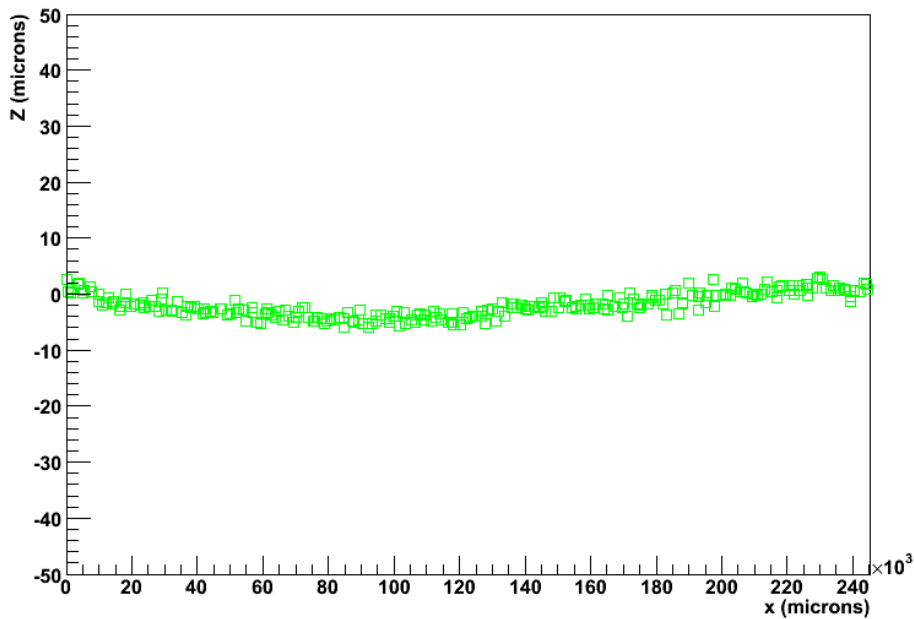


**Figure 30** Difference between measured profiles of a SiC foam ladder at temperatures of 17 C and -8 C.

### ***All-silicon structures***

LCFI work in collaboration with colleagues at FNAL and Washington University has continued. Progress has been made in the investigation of the previously described “all-silicon” vertex detector. First finite-element models of the effects of cable forces on this structure have been produced. A preliminary result, illustrating the 600  $\mu\text{m}$  distortion in a single piece of silicon caused by applying a force to an attached cable, is shown in Figure 31.

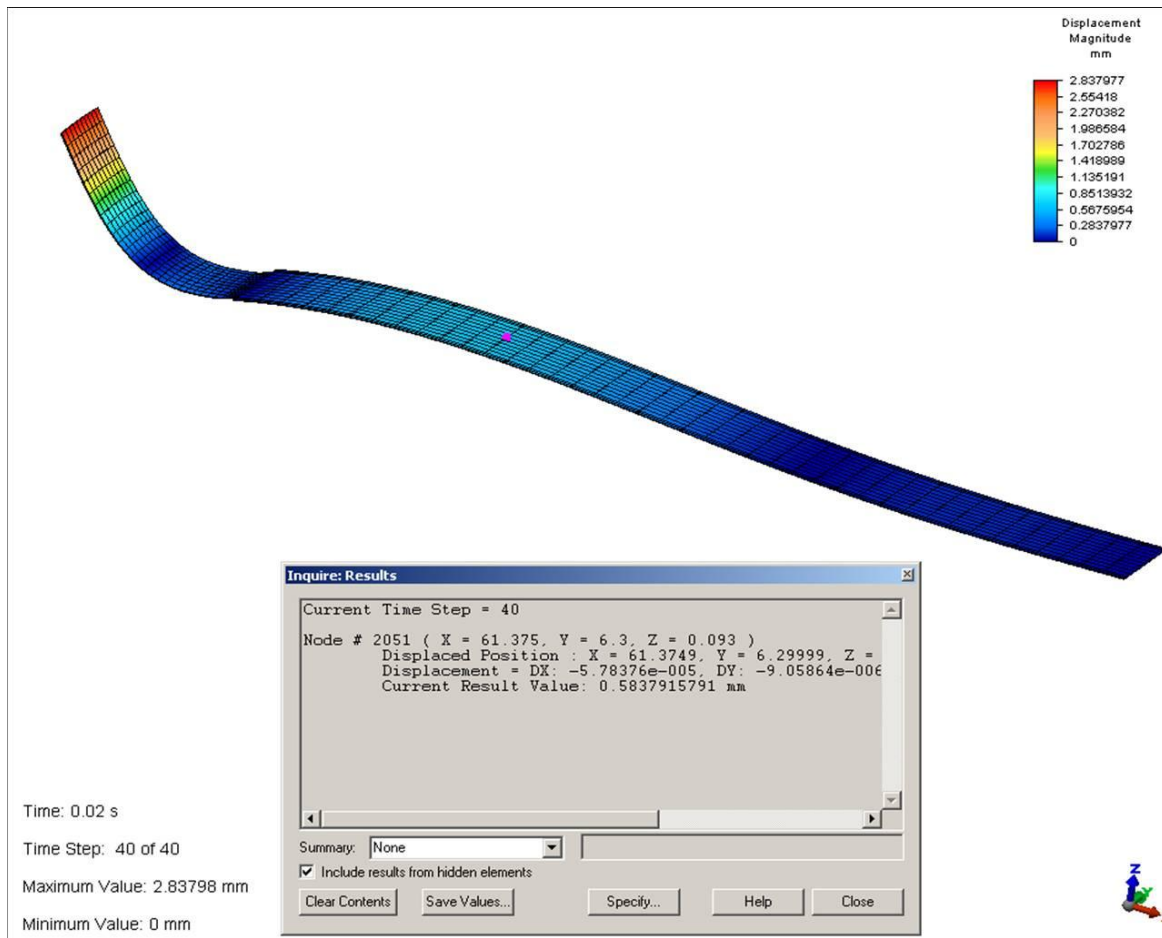


**Figure 31** Distortion of a ladder in an all-silicon vertex detector arising from the forces exerted on the structure by the cables attached at the ladder ends. The position of the maximum displacement is indicated by the pink dot and corresponds to a distortion of about 600  $\mu\text{m}$ .

### ***Other work***

A new minimal-constraint sample holder for the cryogenic survey system has been fabricated and is now in use. This allows more reliable measurements of thermal distortions. An all-SiC support structure for the survey system is also being made and will shortly be available.

### ***Future plans***

Completion of the above studies will bring to an end the LCFI mechanical programme, the results of which will be described in a paper that will be submitted to Nuclear Instruments and Methods.

## WP7 – Test Beams

### *Introduction*

This section of the report describes recent work within the relatively new Work Package 7, in which test beam studies of the LCFI sensors are performed. These form a natural extension of the sensor tests carried out in WP5 (integration and testing). In a beam test, sensor operation is evaluated in an environment that is closer to that in which it will finally be used than is the case in laboratory studies. The main goals of a beam test are the measurement of the efficiency of the sensor and the purity with which clusters can be identified as well as the evaluation of the performance of the complete detector system. Efficiency, the fraction of tracks detected by the sensor, and purity, the fraction of found hits that arise from tracks, can only be measured in a beam test. Other important parameters that can be extracted from test beam data are the position resolution and the amount of charge sharing that occurs between pixels.

### *Results of 2007 beam test*

In June 2007, preparation for the first beam test of ISIS1 started. From the middle of October until the first week of November a successful beam test was performed at DESY (Hamburg) using 6GeV/c electrons. The analysis of this data has been completed. The main results are summarized in Figure 32. For hits occurring around the photogates, the signal-to-noise ratio is  $36.8 \pm 0.2$ . The intrinsic spatial resolution is  $9.4 \pm 0.2 \mu\text{m}$  in the direction of the smaller pixel dimension and the efficiency is 59.3%. The considerable inefficiency and the low signal peak in the cluster signal distribution are due to the asymmetric and large pixel pitch of  $160 \times 40 \mu\text{m}^2$ . In Figure 33, a sketch of the photogate positions is shown. If a hit occurs between two photogates in both the “long” (X) and “short” (Y) directions, the charge is spread over many pixels. In Table 1, the distances between the impact position illustrated in Figure 33 and the photogates marked 1, 2 and 3 are given. Since the charge spreads in proportion to the inverse of the distance, only 6.7% of the charge arrives at each of the photogates marked 1 in the case illustrated. In order to form clusters, hits are required to exceed a threshold of 5 times the noise level. Signals from hits at the location indicated will thus only be combined to form clusters if the signal-to-noise ratio is larger than 75. The actual signal-to-noise ratio, measured for hits close to the photogate, is good, but at  $36.8 \pm 0.2$  is much lower than this value. Hence it is to be expected that the efficiency with the ISIS1 geometry is relatively poor. This feature of the ISIS1 proof-of principle sensor was an inevitable consequence of its construction using the e2v process. In the ISIS2, which has been fabricated by Jazz Semiconductor, the maximum distance to the closest photogate is reduced to  $21 \mu\text{m}$ . This will improve the signal-to-noise ratio and efficiency significantly.

Photogate position	Distance ( $\mu\text{m}$ )	Fraction (%)
1	82.5	6.7
2	100.0	5.5
3	128.1	4.3
4	161.2	3.4
5	197.0	2.8
6	234.1	2.3

**Table 1** Distance to and fraction of total charge arriving at photogates labelled 1, 2 and 3.

The low signal resulting from hits far from the photogates is also observed in simulations of the ISIS1 and a laser scan that was performed at Bristol. In the latter study, light pulses from a 660 nm laser were directed onto the top surface of an ISIS1. The amount of charge deposited was controlled by varying the number of laser pulses used. The total pulse train duration was very short in comparison to the integration time. The pulses were timed such that all signals arrived in memory cell 2. Figure 34 shows the cluster signal distribution as a function of the X and Y coordinates of the motor stage on which the laser was mounted. Clearly visible is the  $160 \times 40 \mu\text{m}^2$  ( $X \times Y$ ) pixel size. The signal resulting from laser pulses far from the photogates is seen to be much lower than that from pulses near the electrodes.

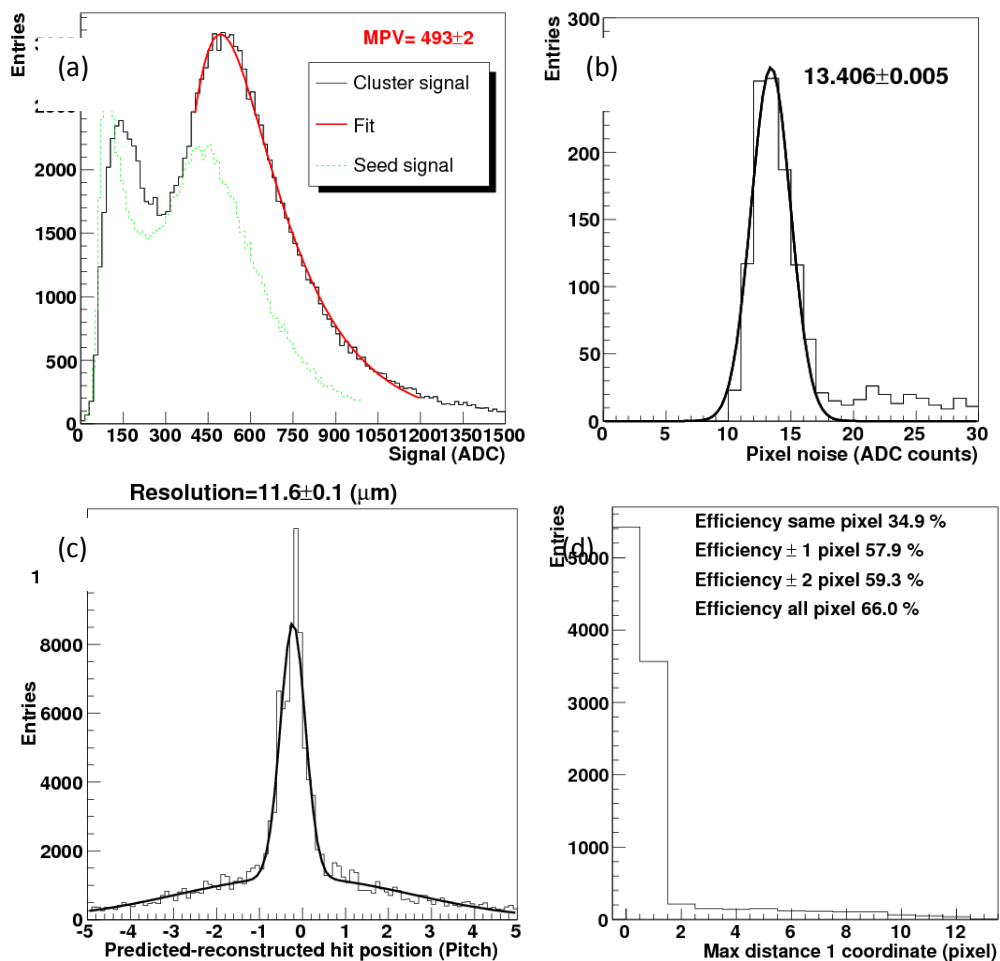


**Figure 32** Summary of main results from first test beam studies of the ISIS1: (a) cluster signal distribution; (b) noise distribution; (c) position residual distribution; (d) number of hits found as a function of the distance between the reconstructed and predicted hit positions.

These results have been presented at various conferences and workshops and have been incorporated in proceedings and in a paper which has been submitted to Nucl. Instr. and Meth A.

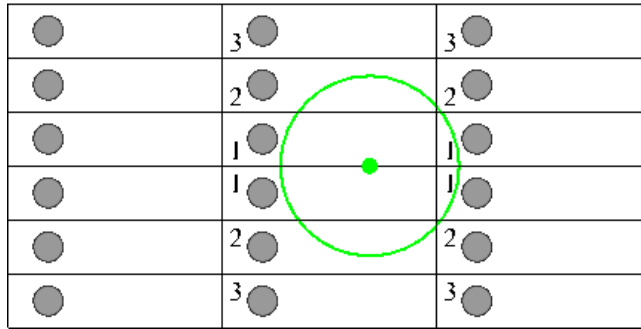


**Figure 33** Sketch to scale of the photogate positions. A hit between the electrodes (filled circle) will share its charge over many pixels. The circle guides the eye to show that the distance between this worst case hit position and the photogates of type 1 is very similar to the distances to photogates of type 2.

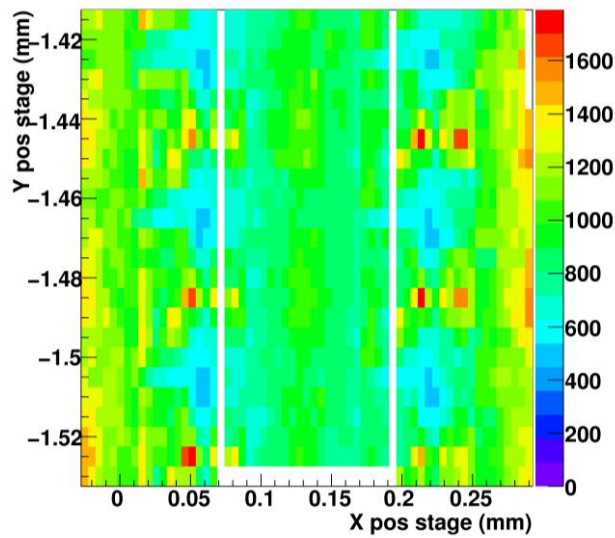


**Figure 34** Cluster signal as a function of the X and Y coordinate of the motor stage. Clearly visible is the  $160 \times 40 \mu\text{m}^2$  pixel structure. Also visible is the decrease in signal with distance from the photogates.

## ***Test beam 2008***

A further beam test was performed in 2008. This took place at CERN at the SPS from August 27<sup>th</sup> until September 3<sup>rd</sup> using a 120 GeV/c pion beam. The EUDET telescope was used to provide an external reference for the beam position. This has two advantages. Firstly, the EUDET telescope has an intrinsic position resolution of  $3 \mu\text{m}$ , resulting in very good precision of the predicted hit positions on the sensors under test. The second advantage is that the EUDET sensors are fully efficient over the entire pixel area. This allows mapping of in-pixel efficiency and signal variations and also removes some of the “quantisation” artefacts that were observed in the 2007 ISIS beam test.

As LCFI had received the p-well ISIS1 devices by the time of the 2008 beam test, these were also studied. These sensors have an extra p-doped layer in the pixel which shields the memory register from the bulk, which should result in a better signal-to-noise ratio. Figure 35 shows that this is indeed the case: the p-well ISIS has a higher signal-to-noise ratio than the standard ISIS when irradiated using an  $^{55}\text{Fe}$  source.

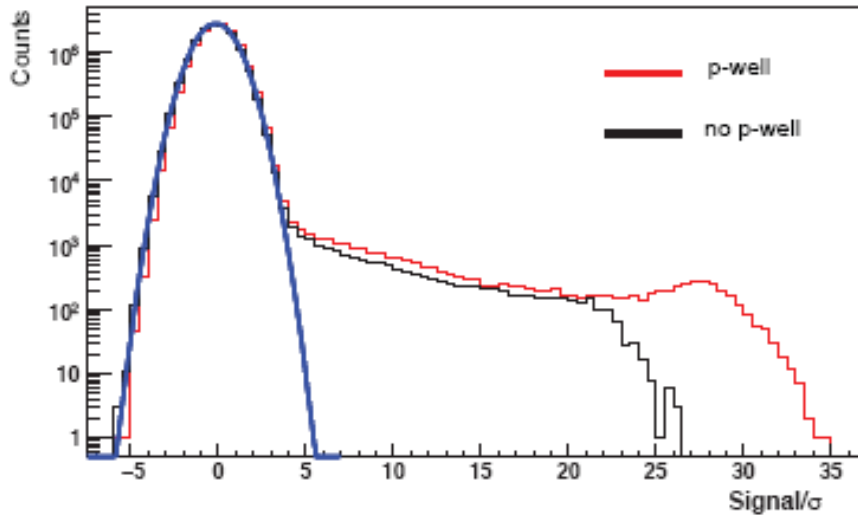


**Figure 35** The signal-to-noise ratio obtained with an  $^{55}\text{Fe}$  source after pedestal correction for both a p-well and a standard ISIS.

Before the beam test, the steering parameters of the two types of ISIS were optimized. As an example of this procedure, the signal-to-noise ratio obtained using an  $^{55}\text{Fe}$  source for both the p-well and standard devices is shown as a function of temperature in Figure 36. The extra p-doped layer indeed shields the memory register, making the noise less leakage-current and hence less temperature dependent.

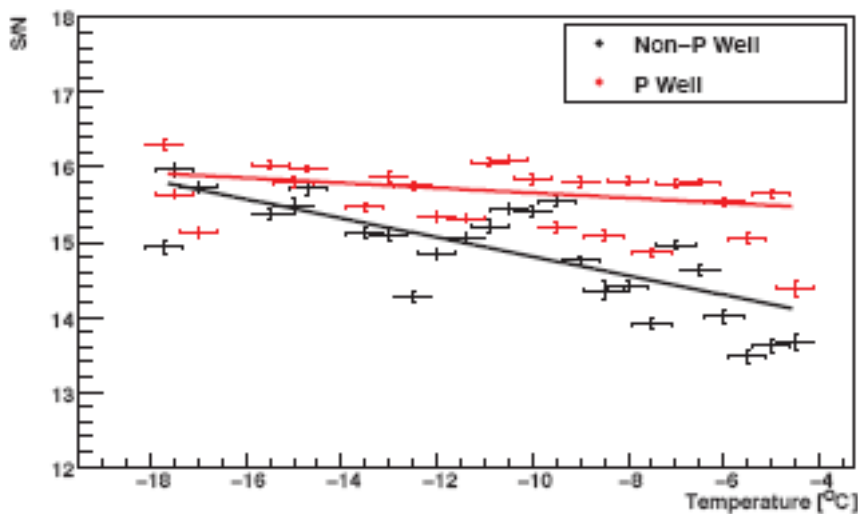


**Figure 36** Signal-to-noise ratio for  $^{55}\text{Fe}$  photons as a function of temperature for ISIS1 devices with and without p-well.

### ***Set-up and first results***

A stack containing 3 p-well and 3 standard sensors was placed in between two stations of the EUDET telescope. A photograph of the set up is shown in Figure 37. The EUDET tracking code was used for the track reconstruction and the sensor alignment. In Figure 38(a), the number of tracks passing the track quality cut per triggered event is shown, while the position resolution of the EUDET planes can be found in Figure 38(b).



**Figure 37** Photograph of the beam test set-up: a stack of 6 ISIS1 devices, 3 p-well and 3 standard, is placed inside a cryostat between 2 EUDET telescope stations.

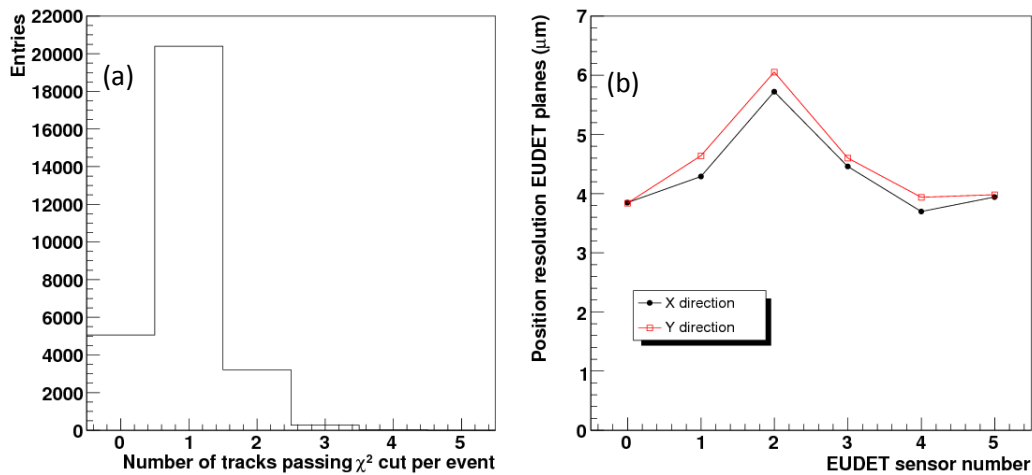


**Figure 38** (a) Distribution of the number of tracks passing the track quality ( $\chi^2$ ) cut per event for a fraction of the data; (b) the sensor position resolution as a function of the plane number.

The analysis of the data taken during the beam test is in its initial stages. Figure 39 shows the signal-to-noise ratio for every pixel in every triggered event during the beam test after pedestal correction. The 3 standard devices are seen to be operating perfectly. Of the p-well devices, ISIS2 shows the expected noise behaviour, but does not seem to detect any beam particles; this was later confirmed using a radioactive source. Signals are observed in both ISIS1 and ISIS2, though in the ISIS1 a couple of pixels are misbehaving and are distorting the shape of the signal-to-noise distribution. There is thus a significant amount of beam test data available for both the standard and p-well sensors.

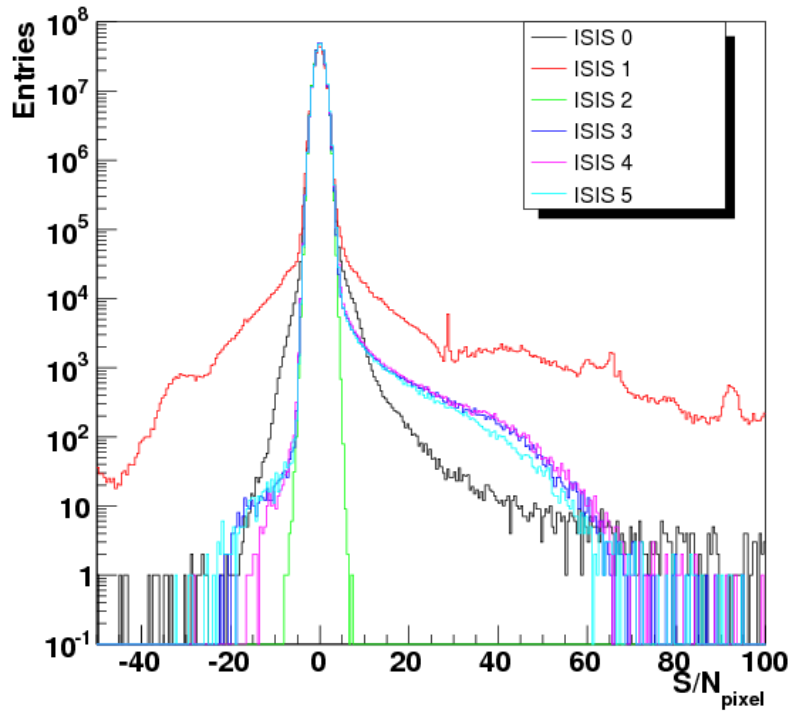


**Figure 39** Signal-to-noise ratio for every pixel in every triggered event during the beam test after pedestal correction. ISIS 0, 1 & 2 are p-well and ISIS 3, 4 & 5 standard devices.

Not only are hits clearly observed in the devices under test, but there are also clear correlations between these and hits in the EUDET sensors. An illustration of this for ISIS5 is found in Figure 40. Here, a hit map for EUDET plane 2 is shown for hits that occur when there was also a hit in the ISIS5. Background was removed by subtracting a hit map generated when there was a hit in the previous event in the ISIS5. Although the plot was made using only a fraction of the available data, the ISIS5 is clearly visible. The geometry of the test set-up dictates that the ISIS5 should show up as a rectangle with about 7 bins on the X-axis and 2 on the Y-axis. Since there are clear hits in all the ISIS devices and there are correlations between the EUDET hits and the ISIS hits, there is strong evidence we have a set of tracks that traverse the ISIS devices of both types. Further analysis is in progress.

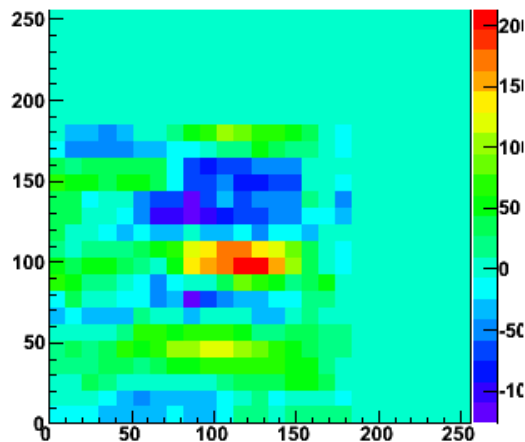


**Figure 40** Background corrected hit map on EUDET plane 2 when a hit occurs in ISIS5.

## **Summary**

The analysis of the 2007 beam test data has been completed. The results have been presented at conferences and workshops and described in a paper which has been submitted for publication.

In late summer 2008, a second beam test was performed. This was carried out at the SPS at CERN using a 120 GeV/c pion beam. Standard and p-well ISIS devices were tested using the EUDET telescope to provide a reference frame. This allows much better tracking than was possible in the 2007 beam test and enables the study of the efficiency and signal charge of the ISIS as a function of the position within the pixel at which the signal was generated.

Analysis of the data taken in the 2008 beam test is in an initial phase, but tracks have already been reconstructed in the telescope, hits in the ISIS sensors found and the tracks successfully correlated with the hits in the EUDET planes. Hence, all the ingredients for a full analysis are present. Currently, work is in progress on the alignment of the ISIS sensors.

# Future Proposals

## ***Introduction***

The three new proposals discussed here, designed to continue the most important and broadly applicable aspects of the LCFI research programme, are being put forward largely by members of the LCFI and CALICE Collaborations, though not all the proposals involve all the members of the two groups. (A further proposal is being written concurrently in which investigations of the design of data acquisition systems based on “off-the-shelf” components are described, but this does not involve LCFI personnel and so is not described here.) These proposals will be presented to the Particle Physics Review Panel at its meeting in Armagh at the end of October.

## ***A silicon pixel detector research programme – SPIDER***

The SPIDER R&D programme aims to establish the viability of monolithic silicon active pixel sensors for future particle physics vertex and tracking detectors and for application in calorimeters. The goal is to investigate the key technical issues involved in the construction of these devices to facilitate the design of application-specific sensors for future experiments. Three devices will be designed and fabricated to study various aspects of these key issues. Their performance will be validated by detailed laboratory measurements and directly in hadron and electron test beams.

The proposal builds on the UK expertise that has been acquired in the last decade or so largely through the work of the LCFI and CALICE Collaborations, but also in the Electronics Department at RAL. Particular features of the sensors that the SPIDER group will investigate include the use of a deep p-well to prevent parasitic charge collection, allowing PMOS electronics to be incorporated in pixels. This approach, pioneered by CALICE in their INMAPS device and LCFI in the ISIS, makes possible sophisticated in-pixel processing without loss of particle detection efficiency. Techniques for the analogue storage of signals in pixel will also be investigated. Again, these studies build on the LCFI development of the ISIS and will result in sensors that have both very high immunity to noise pick-up and low power consumption. A further research direction is the study of pixels with multi-diode geometry which will allow efficient charge collection for the large pixel devices needed for calorimeters with high spatial resolution.

This proposal is being submitted by the Universities of Birmingham and Bristol, by Imperial College London, the University of Oxford and the Rutherford Appleton Laboratory.

## ***Low mass support structures for silicon detectors – LSSD***

The goal of this programme is to further study the potential of materials such as the SiC foams which LCFI has started to investigate for the construction of vertex detectors and tracking systems for future colliders. The proposal covers work for future lepton colliders, such as the ILC or CLIC, but also detectors for future hadron colliders, such as the LHC upgrades, or lepton-hadron colliders, such as the Large Hadron Electron Collider (LHeC). The scope of the studies thus extends beyond the work done by LCFI, both in terms of the scale of the detector structures required, for example central or forward tracking devices are of a much larger size than the LCFI VXD, but also through the necessity of incorporating much increased cooling power, perhaps through the use of evaporative cooling systems. This proposal also aims to complete the measurements of the mechanical properties of foams initiated by LCFI and add to these studies of the thermal properties of foams. Further, Finite

Element Analysis designs of foam structures will be developed and tested, so that reliability of future detector models is assured.

The groups supporting this proposal are from the Universities of Bristol, Glasgow and Liverpool and the Rutherford Appleton Laboratory. The proposed programme will take two years to complete and relies on the use of existing equipment and staff.

### ***Universal flavour identification algorithms for particle physics – FLUID***

The third proposal being submitted aims to further develop vertex and flavour tagging algorithms and to study their application at both lepton colliders in the range of centre-of-mass energies from 0.1 to 10 TeV, that is covering the ILC and CLIC energy range but also energies probably only achievable at a muon collider, and to physics studies at the Large Hadron Collider (LHC) before and after (SLHC) its luminosity upgrade. The concern here is that, while existing algorithms show impressive performance for a limited range of jet energies, that typified by the ILC, they fail to identify b and c quarks with the same efficiency at the very low and very high ends of the jet energy spectrum. Various ideas for improving flavour and charge tagging algorithms have been developed, using advanced analysis techniques and additional information from the calorimeter in the case of lepton linear colliders.

FLUID is being submitted by groups from the Universities of Edinburgh and Oxford.

## Summary

LCFI has continued to make good progress in the last eight months. New results have been obtained on the performance of the proof-of-principle In-situ Storage Image Sensor (ISIS1) device in an electron test beam at DESY. These have conclusively demonstrated that the ISIS is a viable particle detector. A further beam test, using high energy pions at CERN, will provide further results on the performance of the “standard” ISIS, including mapping of efficiencies etc. as a function of the position within the pixel, and first results from the ISIS with deep p-well.

Mechanical studies of foams continue, with the impressive performance achieved with first silicon carbide (SiC) foam prototype ladders being reproduced by new LCFI personnel who have recently started work on the project. SiC foams continue to perform better than Reticulated Vitreous Carbon foams, even when these are compressed to attempt to improve their mechanical properties. First studies of the machining of SiC foams have been performed and are starting to demonstrate the boundaries within which detector designers must operate. Detailed calculations of the stresses imposed on ladders in an all-silicon vertex detector due to the attachment of the cables needed to bring in control signals from, and transfer the data to, the outside world have been performed. The effects are seen to be significant. The tools developed for this study are now available for use on other detector designs.

All the sensors, readout and drive chips designed by LCFI have now been manufactured and all but the second generation ISIS, the ISIS2, have already been delivered to the Collaboration. ISIS2 delivery is expected in the next week or so. Studies of the high speed double-level metal column parallel CCD have demonstrated successful operation with low noise up to frequencies of 25 MHz using the LCFI Column Parallel Drive chip, CPD1. Operation at up to 35 MHz has been possible with this chip, but with increasing noise levels. Studies of LCFI ideas for power and clock amplitude reduction incorporated in the design of the CPC-T test devices have started and have demonstrated that the power required by column parallel and other CCDs can indeed be reduced, though none of the devices tested has yet shown the largest hoped for power reductions.

First tests have shown that the modifications made to the design of the column parallel readout chip CPR2 to produce the CPR2A have had the desired effects. The charge sensitive channels on the chip are working and the cluster finding is now able to cope with higher hit densities. Solutions have thus been developed that demonstrate the feasibility of the column parallel readout of a full scale column parallel CCD-based vertex detector.

Development of the LCFI Vertex Package has continued. A comprehensive round of tuning has been performed, using the latest Monte Carlo simulations and reconstruction packages. It has been demonstrated that the performance of the package continues to be excellent when reconstructed information, for example on photon conversions,  $K_S$  and  $\Lambda$  decays, is used rather than “Monte Carlo truth”. New ideas continue to be incorporated in the package, such as a new method for determining the quark charge and a new algorithm for flavour identification. These offer the potential for future improvements of the software. Studies using the Vertex Package to investigate the precision achievable in the measurement of both Standard Model (e.g. Higgs branching ratios) and new physics processes (e.g. anomalous  $Wtb$  couplings) using the ILD and SiD detectors at the ILC have continued and will feature in the Letters of Intent for the construction of these detectors.

The results mentioned above have been presented at conferences and are in the process of being published in the relevant journals.

In conclusion, LCFI has made significant progress over the last eight months and the Collaboration is now close to completing the research programme it proposed three years ago, despite the recent problems due to the STFC funding crisis. Elements of the programme have been identified as requiring further research, to ensure the ideas developed by LCFI find application in future particle physics detectors. Members of the Collaboration have prepared proposals requesting support for this research that will be presented to the Particle Physics Review Panel later this month.

Finally, we would like to thank the members of the Oversight Committee for the support and guidance they have provided over the last three years; you have helped make this programme the success that it is.

# Appendices

## ***Appendix 1 – LCFI presentations***

Sonja Hillert, “LCFI Vertex Package, parameter optimization”, Joint ACFA Physics and Detector Workshop on the International Linear Collider, March 2008, Sendai, Japan.

Tomáš Laštovička, “Benchmark studies with the LCFI Vertex Package”, Joint ACFA Physics and Detector Workshop on the International Linear Collider, March 2008, Sendai, Japan.

Konstantin Stefanov, “A CCD-based vertex detector”, Joint ACFA Physics and Detector Workshop on the International Linear Collider, March 2008, Sendai, Japan.

Tim Greenshaw “LCFI in 2008”, Linear Collider UK meeting, April 2008, Birmingham, England.

Jaap Velthuis, “LCFI detector overview”, International Linear Collider ECFA workshop, June 2008, Warsaw, Poland.

Roberval Walsh, “Recent developments in the LCFI Vertex Package”, International Linear Collider ECFA workshop, June 2008, Warsaw, Poland.

Sonja Hillert, “The LCFI Vertex Package”, Seventeenth international workshop on vertex detectors, July 2008, Utö Island, Sweden.

Erik Devetak, “Anomalous  $Wtb$  at the ILC – from tools to physics”, Institute of Physics annual particle physics conference, April 2008, Lancaster, England.

Mark Grimes, “Higgs studies at a future electron positron collider”, Institute of Physics annual particle physics conference, April 2008, Lancaster, England.

Ben Jeffery, “LCFI vertex software update”, Institute of Physics annual particle physics conference, April 2008, Lancaster, England.

Talini Pinto Jayawardena, “Realistic reconstruction of top quark pairs for the ILC”, Institute of Physics annual particle physics conference, April 2008, Lancaster, England.

David Cussans, “First test beam results from the ISIS1 detector”, Eight international conference on position sensitive detectors”, September 2008, Glasgow, Scotland.

Steve Worm, “New sensors for particle detection with in-situ charge storage”, Topical workshop of electronics for particle physics, September 2008, Naxos, Greece.

Andre Sopczak, “Modelling of charge transfer inefficiency in a CCD with column parallel readout”, Eleventh topical seminar on innovative particle and radiation detectors, October 2008, Sienna, Italy.

## Appendix 2 – LCFI Risk Register

The LCFI Risk Register is shown in Table 2.

Linear Collider Flavour Identification Risk Assessment 6/10/08											
Owner	Risk description	Potential impact on project	Inherent Prob. (P)	Risk Impact (I)	P x I	Controls	Mitigating factors	Residual Prob. (P)	risk Impact (I)	L x I	Comment / Proposed Action
<b>Risks associated with ILC</b>											
Proj.	Machine design alterations reduce physics possibilities of VXD and hence ILC.	Decreased significance of LCFI project.	2	4	8	Monitor ILC design, oppose inappropriate changes.	Vast majority of ILC detector community similarly opposed to these changes, Ref. Design Report now published.	1	4	4	Successfully opposed aspects of "low P" option.
Proj.	Expected background hit densities in VXD increase significantly.	Pattern recognition becomes problematic using CPCCD.	2	3	6	Detailed studies of backgrounds performed and ongoing, so far without indication of problems.	ISIS significantly more robust as regards pattern recognition.	2	2	4	Monitor ILC background studies, continue development of ISIS, impact here depends on scale of background increase.
Proj.	Expected radiation doses in VXD increase significantly.	Life of CPCCD at ILC significantly shortened.	2	3	6	Detailed studies of radiation doses performed and ongoing.	ISIS more radiation tolerant than CPCCD.	2	2	4	Monitor expected ILC radiation doses, continue development of ISIS, impact depends on amount by which radiation dose increases.
<b>Risks associated with developing ILC collaboration</b>											
Proj.	LCFI sensors not chosen for one of ILC VXD's.	Failure to find place in ILC collaboration and gain access to ILC data.	2	5	10	Effort on physics, mechanical studies and to some extent readout makes LCFI attractive partner in collaboration even if other sensors chosen.	LCFI recognised as one of leading VXD groups.	1	5	5	Continue to publicise LCFI progress on all fronts at ILC meetings. Work on two LoIs.
<b>Risks associated with LCFI funding</b>											
Proj.	Reduction in STFC support for project.	Insufficient resources to complete development of sensors, electronics and support structures and to pursue physics studies, with decrease in likelihood that LCFI can join ILC collaboration.	4	5	20	Ensure good progress with current programme, expose work to international peer review.	Generous STFC support obtained initially, attempts made by STFC to ameliorate effects of funding shortfall.	4	5	20	Attempt to obtain some funding through EU and from STFC for new projects.
<b>Risks associated with LCFI staff</b>											
Proj.	Loss of critical staff or WP leaders.	Experts and leaders become overloaded, delaying progress of project.	2	3	6	Spread expertise through Collaboration, provide interesting and challenging environment with as much autonomy as possible for key staff, ensure smooth handover if WP leaders move to new projects.	None.	3	4	12	Some new skilled staff appointed, but not interested in joining LCFI because of funding situation: some areas understaffed.
<b>Risks associated with physics studies</b>											
WP1	Failure to exploit Vertex Package.	Loss of standing of LCFI.	2	3	6	Adding collaborators, starting physics benchmark studies, collaboration with CALICE.	Many other international groups using and proposing to use Vertex Package.	1	3	3	Add new institutes with interest in physics studies, e.g. Edinburgh.
<b>Risks associated with LCFI sensors</b>											
WP2	Low mass CPD drive cannot be realised.	CPCCD unlikely to be candidate VXD technology.	1	4	4	More effort going to CPD early in project, exploring alternative drive and low voltage/low capacitance CPC designs.	ISIS as alternative if CPCCD fails.	1	2	2	CPD1 largely satisfies requirements.
WP2	Failure or significant delay in CPCCD production run.	Delay in schedule, reduced time for testing.	2	3	6	Close monitoring of production and liaison with manufacturers, increased number of test stands to allow rapid sensor testing.	None.	1	1	1	All CPCs now delivered.
WP2	Failure to produce acceptable design for ISIS.	Lack of alternative sensor to CPCCD if this fails.	2	3	6	Working with designers at Jazz Semiconductor and RAL so alternatives available.	CPCCD tests successful to date.	1	1	1	ISIS2 design complete.
WP2	Delay in ISIS production due to manufacturing difficulties.	Lack of alternative sensor to CPCCD if this fails.	4	3	12	Consulting with several vendors on ISIS construction, including DALSA, Jazz and Lincoln Labs, working with Prof. Etoh Goji. Contract signed with Jazz Semiconductor.	CPCCD tests successful to date.	1	1	1	ISIS2 now manufactured.
WP2	Significant change in exchange rate.	Change in cost if ISIS manufactured overseas.	3	2	6	None.	Pound currently strong.	1	1	1	All contracts now placed.
<b>Risks associated with ASIC production</b>											
WP3	Failure or significant delay of an ASIC production run.	Delay in schedule, reduced time for testing.	4	3	12	Detailed simulation studies performed before submission, close contact maintained with manufacturers during design.	Technologies used so far well proven.	1	1	1	All chips now delivered.
WP3	Significant change in exchange rate.	Change in cost for non-UK items.	3	2	6	None.	Pound currently strong.	1	1	1	All contracts placed.
WP3	Unavailability of multi-project fabrication.	Delay in production, increased cost.	2	2	4	None.	CERN now has MPW plan, RAL utilising vendor-based MPW.	1	1	1	All chips now delivered.

Owner	Risk description	Potential impact on project	Inherent	Risk		Controls	Mitigating factors	Residual	risk		Comment / Proposed Action
			Prob. (P)	Impact (I)	P x I			Prob. (P)	Impact (I)	L x I	
	<b>Risks associated with development of test electronics</b>										
WP4	Problems with vendor or university turn-around time for PCBs.	Delay in testing and feedback to WP2, 3.	3	3	9	New WP manager, involve further group in PCB design, hire further engineer.	None.	1	2	2	All board designs now complete and boards in use or on final testing phase.
	<b>Risks associated with sensor testing</b>										
WP5	Delays in RA appointments due to lack of suitable candidates.	Delay in design and testing of prototypes.	4	3	12	Appointments made at RAL and Bristol, excellent candidate identified for Liverpool post.	None.	3	3	9	Finding good candidates difficult due to attraction of imminent start-up of LHC, many of good applicants resulted from personal contacts.
WP5	Testing site overloaded or inadequate.	Delay in testing and feedback to WP2, 3.	2	3	6	Commission further stands.	None.	3	3	9	Oxford test stand now running and Liverpool test stand inactive due to loss of staff.
WP5	Failure of bump-bonding run.	Delay in module construction and testing.	2	3	6	Switch to alternative vendor of VTT fail to deliver.	VTT have learned from past problems, bump-bonding of CLC2/CPR2 carried out successfully.	1	3	3	Switch would involve delay.
	<b>Risks associated with mechanical studies</b>										
WP6	Failure to find suitable ladder support technology.	Delay in prototype module construction.	2	3	6	Testing new materials for ladders and investigating "shell" structure, new materials promising.	None.	1	3	3	Can compromise on material budget if necessary.
	<b>Risks associated with test beam studies</b>										
WP7	Insufficient resources available for test beam studies.	Inability to test devices in beam.	3	2	6	Working with EUDET to minimise required LCFI resource. First successful test beam runs carried out.	New Bristol appointment expert in test beam studies	1	1	1	Two successful beam tests performed
P = Probability on scale of 1...4, where 1 is low.											
I = Impact on scale of 1...5, where 1 is low.											
Moderate risk (amber) is indicated when $8 \geq P \times I \geq 13$ and high risk (red) when $14 \geq P \times I \geq 20$											

**Table 2** Register of risks with their estimated likelihood, expected consequences and mitigating factors for the LCFI project.

## References

---

<sup>1</sup> <http://lcio.desy.de/>

<sup>2</sup> R. Hawkins, ‘[Vertex detector and flavour tagging studies for the TESLA linear collider](#)’, LC-PHSM-2000-021

<sup>3</sup> A. Hoecker, P. Speckmayer, J. Stelzer, F. Tegenfeldt, H. Voss, K., ‘[TMVA Toolkit for Multivariate Data Analysis with ROOT Users Guide](#)’, arXiv physics/0703039, CERN-OPEN-2007-00;

<sup>4</sup> S. Hillert, ‘ZVMST: a minimum spanning tree-based vertex finder’, submitted as LC-note, July 2008

<sup>5</sup> <http://berggren.home.cern.ch/berggren/sgv.html>

<sup>6</sup> K. Desch, Th. Kuhl, ‘Simulation of Hadronic Branching ratios of a Standard Model like light Higgs Boson at TESLA at 350 GeV’, LC-PHSM-2007-002

<sup>7</sup> <http://sourceforge.net/projects/fann/>